Analysis of Permafrost Thermal Dynamics and Response to Climate Change in the CMIP5 Earth System Models

CHARLES D. KOVEN, WILLIAM J. RILEY, AND ALEX STERN

Lawrence Berkeley National Laboratory, Berkeley, California

(Manuscript received 25 April 2012, in final form 5 September 2012)

ABSTRACT

The authors analyze global climate model predictions of soil temperature [from the Coupled Model Intercomparison Project phase 5 (CMIP5) database] to assess the models' representation of current-climate soil thermal dynamics and their predictions of permafrost thaw during the twenty-first century. The authors compare the models' predictions with observations of active layer thickness, air temperature, and soil temperature and with theoretically expected relationships between active layer thickness and air temperature annual mean- and seasonal-cycle amplitude. Models show a wide range of current permafrost areas, active layer statistics (cumulative distributions, correlations with mean annual air temperature, and amplitude of seasonal air temperature cycle), and ability to accurately model the coupling between soil and air temperatures at high latitudes. Many of the between-model differences can be traced to differences in the coupling between either near-surface air and shallow soil temperatures or shallow and deeper (1 m) soil temperatures, which in turn reflect differences in snow physics and soil hydrology. The models are compared with observational datasets to benchmark several aspects of the permafrost-relevant physics of the models. The CMIP5 models following multiple representative concentration pathways (RCP) show a wide range of predictions for permafrost loss: 2%–66% for RCP2.6, 15%–87% for RCP4.5, and 30%–99% for RCP8.5. Normalizing the amount of permafrost loss by the amount of high-latitude warming in the RCP4.5 scenario, the models predict an absolute loss of 1.6 ± 0.7 million km^2 permafrost per 1°C high-latitude warming, or a fractional loss of 6%–29% $°C^{-1}$.

1. Introduction

Permafrost is a critical component of high-latitude land and determines the character of the hydrology, ecology, and biogeochemistry of the region. There is widespread interest in the use of coupled atmosphere–ocean–land surface models to predict the fate of permafrost over the next centuries because 1) permafrost contains the largest organic carbon (C) reservoir in the terrestrial system (Tarnocai et al. 2009), 2) permafrost stability is primarily dependent on temperature, and 3) global warming is expected to be relatively larger over the permafrost domain because of arctic amplification processes (Holland and Bitz 2003). Thawing of permafrost soils over the next century (Lawrence and Slater 2005) may contribute a powerful greenhouse gas feedback caused by microbial decomposition and release as CO_2 and CH_4 of the frozen-soil C to the atmosphere (Koven et al. 2011; Schaefer et al. 2011). This feedback may also have operated during prior climate warmings (Ciais et al. 2012; DeConto et al. 2012).

Here we analyze output from a set of earth system models (ESMs) (Table 1) that participated in phase 5 of the Coupled Model Intercomparison Project (CMIP5) (Taylor et al. 2009) to evaluate the permafrost model predictions against observations and theoretical expectations and to compare the predicted fate of permafrost under warming scenarios. Because the models participating in this exercise do not include critical process representation needed to calculate the permafrost C budget itself, which at a minimum includes sufficient belowground vertical resolution in their biogeochemical component to distinguish between permafrost and active layer carbon pools (Koven et al. 2009, 2011), we do not attempt to calculate a permafrost C feedback here; instead, we focus on the soil thermal environment and thaw predictions, which are represented in these models

Corresponding author address: Charles D. Koven, Lawrence Berkeley National Laboratory, 1 Cyclotron Rd., MS 50-4037, Berkeley, CA 94720.
E-mail: cdkoven@lbl.gov

DOI: 10.1175/JCLI-D-12-00228.1

TABLE 1. List of models used in this analysis, the modeling groups that developed them, model attributes, and references. The model attributes listed here are relevant to soil physics at high latitudes, including whether the model includes a multilayer snow model, whether the snow acts to insulate between the soil and atmosphere, the inclusion of soil water latent heat and differing frozen- and unfrozen-soil thermal conductivity, and whether soil physical properties are effected by geographically varying soil organic matter.

Model name	Modeling group	Land model	Multiple snow layers	Snow between soil and atmosphere	Latent heat of soil water	Differing frozen/unfrozen soil thermal conductivity	Organic matter	Reference
BCC-CSM1–1	BCC	BCC Atmosphere-Vegetation Interaction Model (BCC_AVIM1.0)	Yes	Yes	Yes	Yes	No	Ji (1995)
CCSM4.0	NCAR	CLM4	Yes	Yes	Yes	Yes	Yes	Lawrence et al. (2011)
CESM1-CAM5	NCAR	CLM4	Yes	Yes	Yes	Yes	Yes	Lawrence et al. (2011)
CanESM2	Canadian Centre for Climate Modelling and Analysis (CCCMA)	Canadian Land Surface Scheme (CLASS)	No	Yes	Yes	Yes	No	Verseghy (1991)
GFDL-ESM with GOLD ocean component (2G)	GFDL	GFDL Land Model 3.0 (LM3.0)	Yes	Yes	Yes	Yes	No	Dunnea et al. (2012)
GFDL-ESM with MOM4 ocean component (2M)	GFDL	GFDL LM3.0	Yes	Yes	Yes	Yes	No	Dunnea et al. (2012)
GISS Model E coupled with Russell ocean model (E2-R)	Goddard Institute for Space Studies (GISS)	GISS Land Surface Model	Yes	Yes	Yes	Yes	Yes	Rosenzweig and Abramopoulos (1997)
HadCM3	Met Office Hadley Centre (MOHC)	MOSES	No	No	Yes	Yes	No	Cox et al. (1999)
HadGEM2-CC	MOHC	MOSES2	No	No	Yes	Yes	No	Essery et al. (2003)
HadGEM2 Earth System (ES)	MOHC	MOSES2	No	No	Yes	Yes	No	Essery et al. (2003)
INM-CM4	INM	INM-CM4	Yes	Yes	Yes	Yes	Yes	Volodin et al. (2010)
IPSL-CM5 Coupled with NEMO (A) Low Resolution (LR)	IPSL	ORCHIDEE	Yes	No	No	No	No	Krinner et al. (2005)
IPSL-CM5A Medium Resolution (MR)	IPSL	ORCHIDEE	Yes	No	No	No	No	Krinner et al. (2005)
MIROC-ESM Chemistry Coupled (CHEM)	Japan Agency for Marine-Earth Science and Technology (JAMSTEC)	Minimal Advanced Treatments of Surface Interaction and Runoff (MATSIRO)	Yes	Yes	Yes	No	No	Takata et al. (2003)
MIROC-ESM	JAMSTEC	MATSIRO	Yes	Yes	Yes	No	No	Takata et al. (2003)
MIROC5	JAMSTEC	MATSIRO	Yes	Yes	Yes	No	No	Takata et al. (2003)
MPI-ESM-LR	Max Planck Institute for Meteorology	JSBACH	Yes	No	No	No	Yes	Raddatz et al. (2007)
MRI-CGCM3	MRI	Hydrology, Atmosphere and Land (HAL)	Yes	Yes	Yes	Yes	No	Yukimoto et al. (2012)
NorESM1-M	Norwegian Climate Centre (NCC)	CLM3	Yes	Yes	Yes	Yes	Yes	Lawrence et al. (2011)

and can thus serve as a basis for calculating the possible range of feedback strength (Schneider von Deimling et al. 2012; Harden et al. 2012; Burke et al. 2012).

The purpose of this paper is twofold: 1) to document the behavior, in comparison with observations, of the permafrost-relevant aspects of these models in the current climate and 2) to compare the model predictions of future changes with permafrost under climate change. By providing a framework for assessing realism of the models, we hope to lay a foundation for benchmarking the frozen-soil physics of these models, which can then serve to inform future development (Luo et al. 2012). By doing this in the context of an intercomparison of future predictions, we seek to analyze how model differences that can be seen in the current climate affect the future response.

A number of authors have developed high-latitude-specific models of the exchange of energy and water to study the behavior of soil freeze and thaw processes. These models were initially developed for local and regional studies (Romanovsky and Osterkamp 1997; Hinzman et al. 1998; Shiklomanov et al. 2007; Rinke et al. 2008; Nicolsky et al. 2009). Many of the relevant processes, including the specific thermal and hydrological properties of organic soils, have been incorporated into global models (Nicolsky et al. 2007; Lawrence and Slater 2008; Schaefer et al. 2009; Koven et al. 2009).

We focus on the CMIP5 models as a representative set of global coupled models that are being used as an integral component of the Intergovernmental Panel on Climate Change Fifth Assessment Report (IPCC AR5). The CMIP5 project included a large number of simulation experiments, including testing model response to a range of forcings, decadal predictability experiments, control scenarios, and paleoclimate experiments. To evaluate the high-latitude thermal predictions of the models, we analyze three representative concentration pathway (RCP) future warming scenarios, RCP2.6, RCP4.5, and RCP8.5, which correspond to 2.6, 4.5, and 8.5 W m^{-2} forcing by 2100, respectively, and thus represent low, intermediate, and high warming scenarios (Taylor et al. 2009). We examine the ability of the CMIP5 models to simulate relevant aspects of the currently frozen soil thermal dynamics and how these dynamics may change under the set of warming experiments. While many such numerical experiments have been conducted using regional permafrost models forced by atmospheric dynamics, it is useful to look to this large, state-of-the-art sample of ESMs, which includes a broad set of climate sensitivities, arctic amplification factors, and detailed land–atmosphere coupling, along with a clearly prescribed experimental design and forcing perturbation, to better understand the range of possible model-predicted permafrost rates under different global warming scenarios.

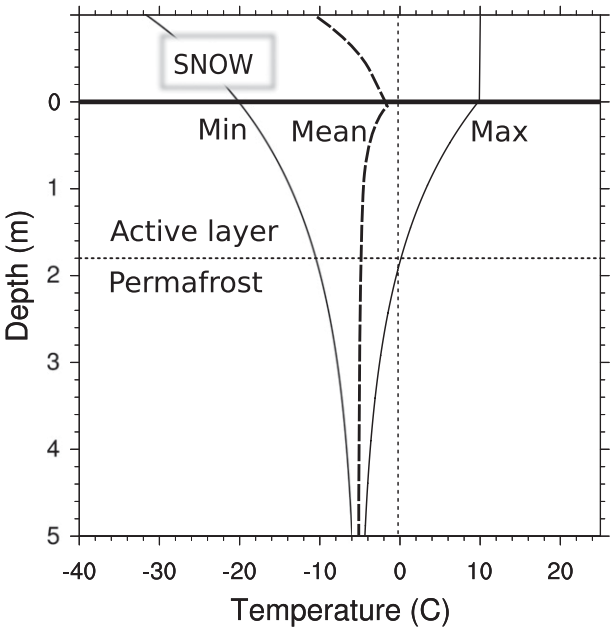

FIG. 1. Simplified schematic of permafrost thermal dynamics. Solid lines show vertical profiles of minimum and maximum annual temperatures; dashed line shows mean annual temperature profile. Snow acts to insulate soils during winter, leading to steep gradient in wintertime and mean temperatures.

A similar analysis, focusing on the changes to the distribution of climatological metrics known to influence permafrost extent, is being conducted by Slater and Lawrence (2013).

A simplified schematic of temperature dynamics for northern soils (Fig. 1) shows that the soil temperature annual cycle is driven by changes in the radiative forcing and surface heat exchange, such that the amplitude of the seasonal cycle is greatest in the air, decreases across the air–soil interface, and decreases further with depth into the soils following a roughly exponential profile. The active layer in permafrost soils is defined as the maximum depth at which the annual temperature wave causes the soil to thaw on a regular basis (at least every other year). Coupling among environmental conditions, thermal properties, phase change, ground ice, and cryoturbation make the actual temperature dynamics of permafrost soils more complex than can be represented by simple diffusive energy transport. Across the air–soil interface, snow acts to insulate during the winter but not during the summer, leading to thermal rectification and warmer mean soil temperatures than mean air temperatures. Within the soil column, the low thermal diffusivity of organic soil horizons and the large amount of latent heat required to freeze and thaw moisture in the active layer leads to rapid attenuation of the annual temperature wave. In addition, the differences between frozen and thawed soil thermal conductivities, particularly

for organic soils, which are good insulators in the summer but allow heat to escape during the winter, lead to further change in the mean temperatures with depth, though with a cooling rather than a warming effect (Romanovsky and Osterkamp 1997).

The CMIP5 models represent these processes very differently, both conceptually and numerically. For example, snow insulation may be treated either as a separate layer or layers existing above the soil column [''bulk'' or ''multilayer'' snow schemes in the classification of Slater et al. (2001)] or as a transient replacement of the upper soil column with snowlike properties [''composite'' or ''implicit'' schemes (Slater et al. 2001)]. The representation of soil physical properties differs greatly as well, with some models including the effects of organic matter [e.g., those with Community Land Model, version 4 (CLM4), as their land model: Community Climate System Model, version 4.0 (CCSM4.0); Community Earth System Model, version 1–Community Atmosphere Model, version 5 (CESM1-CAM5); and Norwegian community ESM (NorESM)], while the majority analyzed here use only mineral soil properties. The coupling between thermal and hydrologic states in the models differs as well, with some models not including a latent heat term for soil moisture freeze–thaw processes. The model vertical discretization for soil thermal calculations varies widely between these models as well, as do the mechanics of coupling between the land surface and atmosphere. However, rather than enumerating the differences between the models, our focus here is on diagnosing the net behavior of the different models under current conditions and how that behavior is linked to their predictions of permafrost thaw over the twenty-first century.

2. Methods

a. Analysis of CMIP5 models

We calculate the active layer thickness (ALT) from the model predictions using monthly mean soil temperatures T_s. Some models in the CMIP5 experiment do not report depth-resolved soil temperatures, and thus, we do not include those models in this analysis. We calculate monthly mean thaw depth as the deepest point in the soil column of a given grid cell at a given month with soil temperature at or above freezing. Given the coarse vertical discretization of land surface models, thaw depth can be defined multiple ways, for example, as the lower edge of the deepest thawed layer (Lawrence and Slater 2005) or, alternatively, by interpolating soil temperature between model level centers and calculating the depth that the interpolated line intersects the freezing point (Lawrence et al. 2012). Here we use the former (level edge) approach and define the freezing point as 0°C. The use of this single temperature threshold may introduce errors in some models because of artifacts in their latent heat parameterizations; this will be discussed in more detail below. We then calculate annual ALT as the maximum monthly thaw depth for a given year. We define permafrost to be present in a grid cell if the maximum annual ALT is shallower than either 3 m or the deepest model soil level, whichever is less; this approach therefore gives a metric of ''near surface'' permafrost (Lawrence and Slater 2005).

To diagnose controls on permafrost distribution within the models, we compare modeled ALT with the local climate. Here we use the monthly mean modeled surface air temperature and examine two quantities that we hypothesize control permafrost distribution in the models: the annual mean temperature and the amplitude of its seasonal cycle. In particular, we are interested in how the propagation of energy in the soil leads to vertical differences in the annual mean- and seasonal-cycle amplitude of soil temperatures. To examine the amplitude of the seasonal cycle, we use a Fourier analysis to calculate the amplitude of the annual frequency of the monthly mean surface air temperature and soil temperature at 0- and 1-m depth. At mid- and high latitudes, the majority of the variance is contained in the annual wave (Stine et al. 2009), so we neglect higher-frequency components. For all model runs, we use the first 10 years of the RCP4.5 climate scenario (2006–15) for this analysis in order to compare against recent observations and average across multiple ensemble members where possible.

For each model, we calculate the change in mean temperature and the amplitude of the seasonal cycle across two vertical gradients: the atmosphere to shallow soil interface and the change from 0- to 1-m depth. Separating the atmosphere to deeper soil thermal connection into these two gradients has the advantage that we can isolate the processes operating across each region. The seasonal-cycle response across the air-to-soil surface interface is mediated by snow insulation, radiative processes, and coupling between the atmospheric boundary layer and the soil surface. The shallow-to-deeper soil gradient is dominated by soil hydrology, latent heat, and thermal properties. An exception to this is for some models that place snow insulation effects within the soil column. Similarly, while the mean temperature and the amplitude of the seasonal cycle will be linked at a given position along these vertical gradients, varying process representation in different models may lead to different levels of thermal rectification associated with the multiple processes operating across each gradient.

The soil vertical grids differ between models. So, to compare them, we need to interpolate predicted T_s to a uniform reference depth. To do this, we assume that the seasonal-cycle T_s amplitude will attenuate roughly

exponentially (Fig. 1), while vertical differences in mean T_s will be roughly linear. Thus, we log transform the temperature amplitude so that it will be roughly linear with depth, then interpolate to the 1-m reference depth and take its exponential. For mean temperatures we perform a simple linear interpolation to 1-m depth. The mean temperature differences are calculated as

$$\Delta\overline{T}_{0\mathrm{m}-1\mathrm{m}} = \overline{T}_{1\mathrm{m}} - \overline{T}_{0\mathrm{m}} \quad \text{and} \tag{1}$$

$$\Delta\overline{T}_{\mathrm{air}-0\mathrm{m}} = \overline{T}_{0\mathrm{m}} - \overline{T}_{\mathrm{air}}, \tag{2}$$

where $\overline{T}_{1\mathrm{m}}$, $\overline{T}_{0\mathrm{m}}$, and $\overline{T}_{\mathrm{air}}$ are the mean temperatures at 1 m, the uppermost soil layer, and air, respectively. We use the uppermost model soil layer as an approximation for the 0-m depth because the top soil layer is very thin for these models. We report the seasonal-cycle amplitude attenuations, $\alpha_{0\mathrm{m}-1\mathrm{m}}$ and $\alpha_{\mathrm{air}-0\mathrm{m}}$, as

$$\alpha_{0\mathrm{m}-1\mathrm{m}} = \frac{\hat{T}_{1\mathrm{m}}}{\hat{T}_{0\mathrm{m}}} \quad \text{and} \tag{3}$$

$$\alpha_{\mathrm{air}-0\mathrm{m}} = \frac{\hat{T}_{0\mathrm{m}}}{\hat{T}_{\mathrm{air}}}, \tag{4}$$

where $\hat{T}_{1\mathrm{m}}$, $\hat{T}_{0\mathrm{m}}$, and $\hat{T}_{\mathrm{air}}$ are the corresponding amplitudes of the seasonal cycle.

b. Analysis of site observations

To compare modeled active layers with observations, we use two ALT datasets: the Circumpolar Active Layer Monitoring (CALM) network (Brown et al. 2000) and a separate analysis of historical ALT derived from soil temperature measurements at 31 Russian sites (Zhang et al. 2006). We also compare modeled soil temperatures directly with observations of soil temperatures using two datasets: 1) the International Polar Year Thermal State of Permafrost (IPY-TSP) (Romanovsky et al. 2010; Romanovsky 2010) and 2) the historical Russian soil temperature (HRST) (Gilichinsky et al. 1998; Zhang et al. 2001).

The IPY-TSP data are measured at multiple depths; here we use only sites that have at least one complete annual cycle at three depths between the surface and 1.5 m. The HRST data are measured at a variety of depths, but the majority of sites have 20 cm as their shallowest depth. The mean temperatures generally show a linear relationship and the seasonal-cycle amplitudes an exponential relationship with depth, allowing interpolation to the reference levels. For both soil temperature datasets where temperature is not reported at the levels of interest (0 and 1 m), we perform a linear regression of the mean temperatures as a function of depth and project it to 0 and 1 m. For the annual cycle amplitudes, we use the same approach but with log-transformed amplitudes.

An important caveat needs to be taken into account with regard to the HRST data. These measurements were generally made on bare soils in which surface organic layers had been removed (Gilichinsky et al. 1998); thus, we expect these observations to underestimate the magnitude of the seasonal-cycle attenuation and cooling with depth for these soils. These patterns are evident in the means for the two data collections: the mean $\Delta\overline{T}_{0\mathrm{m}-1\mathrm{m}}$ for the IPY-TSP data is −0.66°C versus −0.31°C for the HRST data, while the mean $\alpha_{0\mathrm{m}-1\mathrm{m}}$ is 0.38 for the IPY-TSP data and 0.45 for the HRST data. However, we use both datasets here because their spatial domains are different and complementary; the HRST observations are all in Russia, while the IPY-TSP data have panarctic coverage but are focused in Alaska. The difference in spatial coverage is similar for the two active layer datasets: CALM has a broad coverage but little representation of interior Siberia, while the Zhang et al. (2006) data are focused on interior Siberia.

We compare both the active layer and soil temperature data with atmospheric temperature data. Many of the IPY-TSP sites report measurements of the local surface air temperature. We use these data where available and otherwise use climatological means and seasonal cycles in air temperature from the corresponding grid cell of the Climatic Research Unit (CRU) time series 3.1 (TS3.1) surface air temperature climatology (Mitchell and Jones 2005).

3. Results and discussion

a. Comparison of high-latitude soil thermal dynamics under current climate

Simulated current-climate permafrost extent varies widely across the models and between the models and the observation-based map of Brown et al. (1998) (Fig. 2). Since the models generate their own atmospheric climatology, which could partly explain differences in permafrost area, we also show the position of the 0° isotherm in the surface mean annual air temperatures (MAAT, blue line) for each of the models and, in the observations (final) panel, the CRU data. The permafrost distributions of Brown et al. (1998) contain 11.0 and 4.3 million km^2 of continuous and discontinuous permafrost, respectively, for a total of approximately 15.3 million km^2. The models calculate widely divergent total permafrost area under current climate (Table 2). If it were the case that the permafrost differences were caused by differences in predicted climate, the models would show

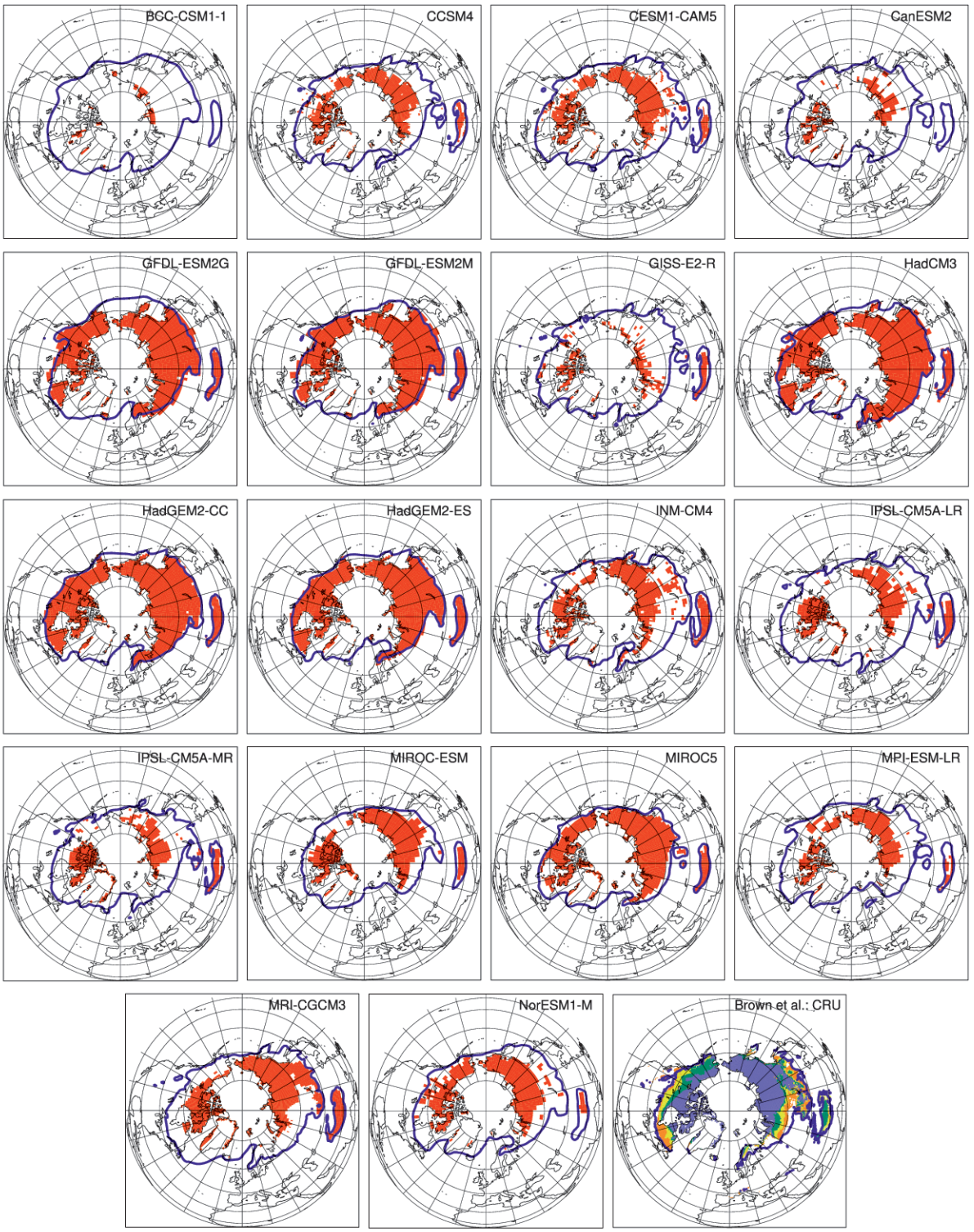

FIG. 2. Extent of permafrost for each of the CMIP5 models under the current climate (using years 2005–15 from the RCP4.5 scenario) as well as for the map of Brown et al. (1998). Also shown in thick blue lines are the 0° isotherm in MAAT for each of the models over the same time period and from the CRU dataset in the observations panel.

a similar spacing between the permafrost edge and the 0° isotherm. Instead, this spacing varies widely between the models, indicating that the differences in permafrost extent lie fundamentally in the modeled soil thermal regimes or in the atmosphere to soil energy exchanges.

In addition to total permafrost area, another crucial component of a given model's permafrost dynamics is the predicted active layer depths. The simple permafrost temperature schematic (Fig. 1) suggests that a model's predicted active layer at a given location should be controlled by the mean annual air temperature and the amplitude of the seasonal cycle, with warmer locations or larger seasonal cycles corresponding to deeper active layers. Figure 3 shows these relationships for each of the models and also for the combined active layer (Brown et al. 2000; Zhang et al. 2006) and atmospheric climatology (Mitchell and Jones 2005). The majority of models show a positive relationship between warmer climate and larger-amplitude seasonal cycles with deeper active layers, although the slopes of these relationships, as well as the fraction of total ALT variance explained by climate, differ between the models and between the models and the observations. As a simple first-order approximation of the relative role of climate in determining ALT between the models, we regress the variables, assuming a relationship of the form

$$Z_{\text{thaw}} = a\overline{T}_{\text{air}} + b\hat{T}_{\text{air}} + c, \tag{5}$$

where Z_{thaw} is the active layer thickness and $\overline{T}_{\text{air}}$ and $\hat{T}_{\text{air}}$ are the mean- and seasonal-cycle amplitudes of surface air temperature. While the observations are consistent with the general relationships (Table 3), the air temperature accounts for a much smaller fraction of total variance ($r^2 = 0.13$) than it does for the simulations ($r^2 =$ 0.22–0.84, with mean of 0.5). Thus, the observations support the idea that factors other than climate, likely including soil conditions and finescale hydrology, account for a large fraction of this variance, while the models, which do not include these finescale controls, attribute too much of the ALT variance to climate. However, for this analysis, we have restricted the ALT observations only to high-latitude sites, which may bias our results away from a climate control since doing so excludes the low-latitude, high-altitude ALT sites, which do show a stronger climate control. Several of the models show a convex-downward trend to the active layer thickness with increasing temperature or a bimodal regime with a shallow cold permafrost slope and a steeper warm permafrost slope. Those with a distinct bimodal slope regime [e.g., Canadian Earth System Model (CanESM); Hadley Centre Coupled Model, version 3 (HadCM3); and Hadley Centre Global Environmental Model, version 2 (HadGEM2)] all have relatively fewer model levels, suggesting that this pattern is an artifact of their limited vertical resolution.

Analytical solutions exist for the 1D heat conduction with phase change that is subject to periodic upper-boundary condition problems, given simplifying assumptions like the Stefan equation (which assumes that frozen soil is initially at 0°C and that the latent heat of fusion dominates the heat budget) and the Kudryavtsev equation (which allows an initial permafrost mean annual temperature less than 0°C) (Romanovsky and Osterkamp 1997; Riseborough et al. 2008). For qualitative comparison, we include panels in Fig. 3 with the predicted active layer from these two equations given a single set of reasonable soil physical parameters (unfrozen soil conductivity = 0.6 W m^{-1} K^{-1} and porosity = 0.25, assuming saturated soils) and climate parameters (we use a simplified climate representation for this exercise: CRU climatological $\overline{T}_{\text{air}}$ and $\hat{T}_{\text{air}}$, assuming a uniform 3° thermal offset $\Delta\overline{T}_{\text{air}-0\text{m}}$, no thermal offset $\Delta\overline{T}_{0\text{m}-1\text{m}}$, and a uniform attenuation coefficient $\alpha_{\text{air}-0\text{m}}$ of 0.6). The Kudryavtsev equation shows the same basic pattern that the numerical models are capturing, that is, active layers increase steeply near the permafrost edges, there is a concave-downward profile between ALT and MAAT, and there is increasing ALT with increasing seasonal-cycle amplitude. For the set of parameters applied here, the Kudryavtsev equation ALT is shallower than predicted in the CMIP5 models, although other parameter choices can lead to deeper ALT while maintaining the same functional form. In contrast, the Stefan equation predicts generally larger ALT than predicted by the Kudryavtsev equation and a slightly concave-upward profile. Thus, the more complex Kudryavtsev equation supports those models that predict 1) smooth concave-downward profiles and 2) clear impacts of the temperature seasonal cycle amplitude and mean on ALT. Further, the Kudryavtsev equation supports the large observed variability in ALT resulting from site-specific differences in soil and snow physical properties.

The distributions of ALT and permafrost area under historical, current, and future climates vary greatly between the models (Fig. 4). This statistic of cumulative ALT distributions is relevant to calculating the C feedback effect associated with permafrost thaw, as the difference between successive curves under a climate warming scenario is proportional to the soil volume transferred from permafrost to active layer and thus the quantity of organic carbon made vulnerable to decomposition as a result of thawing (Harden et al. 2012). Most of the models show ALT distributions under future climate scenarios with a shape roughly the same (though with smaller total magnitude) as under current climate, though some models [e.g., Geophysical Fluid Dynamics Laboratory ESM

TABLE 2. Modeled current and future permafrost extent in the upper 3 m of soil. For qualitative comparison, the 50% of models with the least bias for the present time period are noted in boldface type.

	Historical			RCP4.5				
Model name	PF area 2005 ($\times 10^6$ km^2)	PF area 1850 ($\times 10^6$ km^2)	Fraction PF lost 1850–2005 (unitless)	PF area 2050 ($\times 10^6$ km^2)	Fraction PF remaining 2005–50 (unitless)	PF area 2100 ($\times 10^6$ km^2)	Fraction PF remaining 2005–2100 (unitless)	Global warming 2005–2100 (°C)
BCC-CSM1–1	1.4	2.7	0.47	0.9	0.66	0.8	0.58	1.2
CCSM4.0	**10.5**	13.1	0.20	8.0	0.76	5.7	0.54	1.2
CESM1-CAM5	**12.3**	13.8	0.11	9.1	0.74	6.1	0.49	2.0
CanESM2	3.2	5.7	0.43	0.9	0.29	0.5	0.14	1.9
GFDL-ESM2G	25.6	27.3	0.06	23.5	0.92	22.0	0.86	0.7
GFDL-ESM2M	24.3	27.0	0.10	21.1	0.87	20.0	0.82	0.8
GISS-E2-R	4.5	8.2	0.45	2.6	0.58	2.5	0.57	0.9
HadCM3	27.3	28.6	0.05	—	—	—	—	—
HadGEM2-CC	25.1	24.6	−0.02	20.6	0.82	17.1	0.68	2.0
HadGEM2-ES	22.3	23.4	0.05	17.8	0.80	14.5	0.65	2.1
INM-CM4	**14.0**	15.6	0.11	12.8	0.92	11.5	0.82	1.1
IPSL-CM5A-LR	**12.6**	18.5	0.32	8.5	0.68	7.0	0.56	1.8
IPSL-CM5A-MR	**10.1**	14.9	0.32	6.5	0.64	4.6	0.46	1.8
MIROC-ESM	**11.5**	12.6	0.08	7.3	0.63	4.7	0.40	2.1
MIROC5	**17.4**	19.0	0.08	14.5	0.83	12.3	0.70	1.3
MPI-ESM-LR	8.6	13.7	0.37	6.2	0.72	4.0	0.46	1.3
MRI-CGCM3	**15.5**	16.7	0.08	13.2	0.86	10.9	0.70	1.5
NorESM1-M	**13.3**	15.1	0.11	10.2	0.77	7.3	0.55	1.5
Observations	15.0	—	—	—	—	—	—	—

(GFDL-ESM) and Model for Interdisciplinary Research on Climate, version 5 (MIROC5)] show an increase in the relative abundance of deeper active layers, presumably related to a slowed transient downward thaw. Almost all models predict that some permafrost has already thawed during the twentieth century (the difference between 2005–10 and 1850–59 curves at 3-m depth in Fig. 3), varying between 3% gain [HadGEM2 carbon cycle (CC)] and 49% loss [Beijing Climate Center Climate System Model, version 1–1 (BCC-CSM1–1)] in permafrost area. While it is not clear how much permafrost thaw has occurred during the twentieth century, observations do not support permafrost losses on the high end of this spectrum (Burn and Nelson 2006).

Although the available ALT observations are not evenly distributed throughout the permafrost region and thus are not available as a quantitative comparison against model predictions, we include the cumulative distributions from the observational datasets as a qualitative reference for the overall shape of these distributions. The observations show a broad range of active layer depths, though unlike the models, none of the sites have mean ALT less than ~20 cm; however, this may again be caused by sampling bias avoiding the coldest environments where ALT approaches zero.

Many of the models show steplike distributions in ALT (Fig. 4) associated with the boundaries between the model levels of their finite-difference discretizations. These steplike patterns result from a tendency of a given model level to get stuck at 0°C because of the large latent heat threshold required to transform the entire soil level's mass across the freeze–thaw boundary. In addition, some of the models show unrealistic behavior with respect to shallow active layers, with either too much [e.g., Institute of Numerical Mathematics Coupled Model, version 4 (INM-CM4)] or too little [e.g., the low-resolution Max Planck Institute Earth System Model (MPI-ESM-LR); CanESM, version 2 (CanESM2); and L'Institut Pierre-Simon Laplace Coupled Model, version 5 (IPSL-CM5)] of the permafrost area having shallow active layers. As discussed below, these biases are related to differences in the prescription of the latent heat of fusion of soil water for the models. Differences between the models' ALT predictions can be roughly quantified by calculating the model's median ALT, which varies from almost zero to >3 m (Table 3). While the nonrandom spatial distribution of ALT observations does not allow us to calculate a rigorous observational constraint, the definition of gelisols (permafrost-affected soils) used in USDA Soil Survey Staff (1999) of less than 1 m (or 2 m if other evidence such as cryoturbation is present) rules out plausible values far outside of this range, such as 0.015 m in INM-CM4 at one extreme or 2.6–3.2 m for the IPSL-CM4 or MPI-ESM models at the other extreme.

TABLE 2. (*Extended*)

RCP4.5				RCP2.6		RCP8.5	
High-latitude warming 2005–2100 (°C)	Arctic amplification (unitless)	Total loss PF/degree high-latitude warming ($\times 10^6$ km^2 °C^{-1})	Fractional loss PF/degree high-latitude warming (% °C^{-1})	PF area 2100 RCP2.6 ($\times 10^6$ km^2)	Fraction PF remaining 2005–2100 (unitless)	PF area 2100 ($\times 10^6$ km^2)	Fraction PF remaining 2005–2100 (unitless)
2.7	2.3	0.2	15.4	—	—	0.5	0.36
2.1	1.7	2.3	21.8	7.7	0.73	2.7	0.26
4.2	2.1	1.5	12.1	7.9	0.64	2.4	0.19
4.1	2.2	0.7	20.8	1.1	0.34	0.0	0.01
1.5	2.2	2.3	9.1	25.1	0.98	15.3	0.60
1.2	1.5	3.5	14.3	22.1	0.91	14.8	0.61
1.4	1.5	1.4	31.0	4.4	0.98	1.0	0.23
—	—	—	—	—	—	—	—
5.2	2.6	1.5	6.2	—	—	9.4	0.38
5.3	2.6	1.5	6.5	17.5	0.78	7.0	0.31
2.3	2.2	1.1	7.7	—	—	9.8	0.70
3.4	1.9	1.7	13.2	9.8	0.78	2.0	0.16
3.5	1.9	1.6	15.7	8.1	0.80	1.4	0.14
5.0	2.4	1.4	11.8	6.4	0.55	0.6	0.05
3.3	2.5	1.5	8.9	14.2	0.81	6.5	0.37
2.6	2.0	1.7	20.3	6.9	0.80	0.5	0.06
3.0	2.0	1.5	9.8	12.7	0.82	7.7	0.50
4.1	2.8	1.5	11.1	9.7	0.73	3.5	0.27
—	—	—	—	—	—	—	—

The models occupy different subsets of the possible phase space between climate and ALT (Fig. 3). If a given model's ALT equilibrates rapidly to a change in climate, then time trajectories of ALT in individual grid cells as a function of climate would have comparable slopes to the relationship between comparable climatic conditions across space (i.e., a ''space for time'' relationship). We qualitatively searched for such a relationship in the models by plotting lines connecting the predicted current (2005–10) and future (2090–99 for RCP4.5) ALT (Fig. 5). Across the models, the slopes of these time trajectories are similar to those across space under current climate (Fig. 3), suggesting that the models rapidly equilibrate their predicted ALT to a new climate, at least relative to the centennial time scale used to calculate these differences. The implication of this is that models which show a high sensitivity of current-day climatic control of ALT will also show a high sensitivity of ALT to warming. Since the models tend to overestimate, relative to the observations, both the slope of the spatial MAAT–ALT relationship and the fraction of ALT variance explained by climate (Table 3), it may be that the models are thus too sensitive in their predicted ALT response to climate change.

To diagnose the thermal dynamics responsible for the differences between the CMIP5 models under current climate (2006–15) and to evaluate which models have a more realistic permafrost response to climate warming, we next discuss an analysis of how the models propagate temperature from the air through the upper soils, using the metrics discussed above: $\Delta\overline{T}_{\mathrm{air-0m}}$, $\Delta\overline{T}_{\mathrm{0m-1m}}$, $\alpha_{\mathrm{air-0m}}$, and $\alpha_{\mathrm{0m-1m}}$ in Figs. 6–9.

The majority of models show a positive thermal offset ($\Delta\overline{T}_{\mathrm{air-0m}}$, Fig. 6) over the high-latitude region, which is linked to the strong attenuation of the seasonal-cycle amplitude ($\alpha_{\mathrm{air-0m}}$, Fig. 7). As discussed above, the warming and attenuation are primarily caused by the presence of snow, which can be seen in the models since this effect is confined mainly to the boreal and arctic regions, with a maximum that generally spans the boreal belt. The magnitude of the warming differs between models, with mean $\Delta\overline{T}_{\mathrm{air-0m}}$ at the grid cells corresponding to observations of −0.2°–8.8°C and mean $\alpha_{\mathrm{air-0m}}$ of 0.29–1.05. The two statistics of $\Delta\overline{T}_{\mathrm{air-0m}}$ and $\alpha_{\mathrm{air-0m}}$ are highly correlated between the models, with an $r^2 = 0.8$. Across the air–soil interface, the observations also show a pronounced warming (mean $\Delta\overline{T}_{\mathrm{air-0m}}$ of 6.2°C) in the mean temperatures for the shallowest soils relative to the surface air temperatures and significant attenuation (mean $\alpha_{\mathrm{air-0m}} = 0.57$) of the annual cycle.

Between the shallow and deeper soils, the models show a much smaller temperature gradient ($\Delta\overline{T}_{\mathrm{0m-1m}}$, Fig. 8), and 12 of 19 show a general cooling with depth.

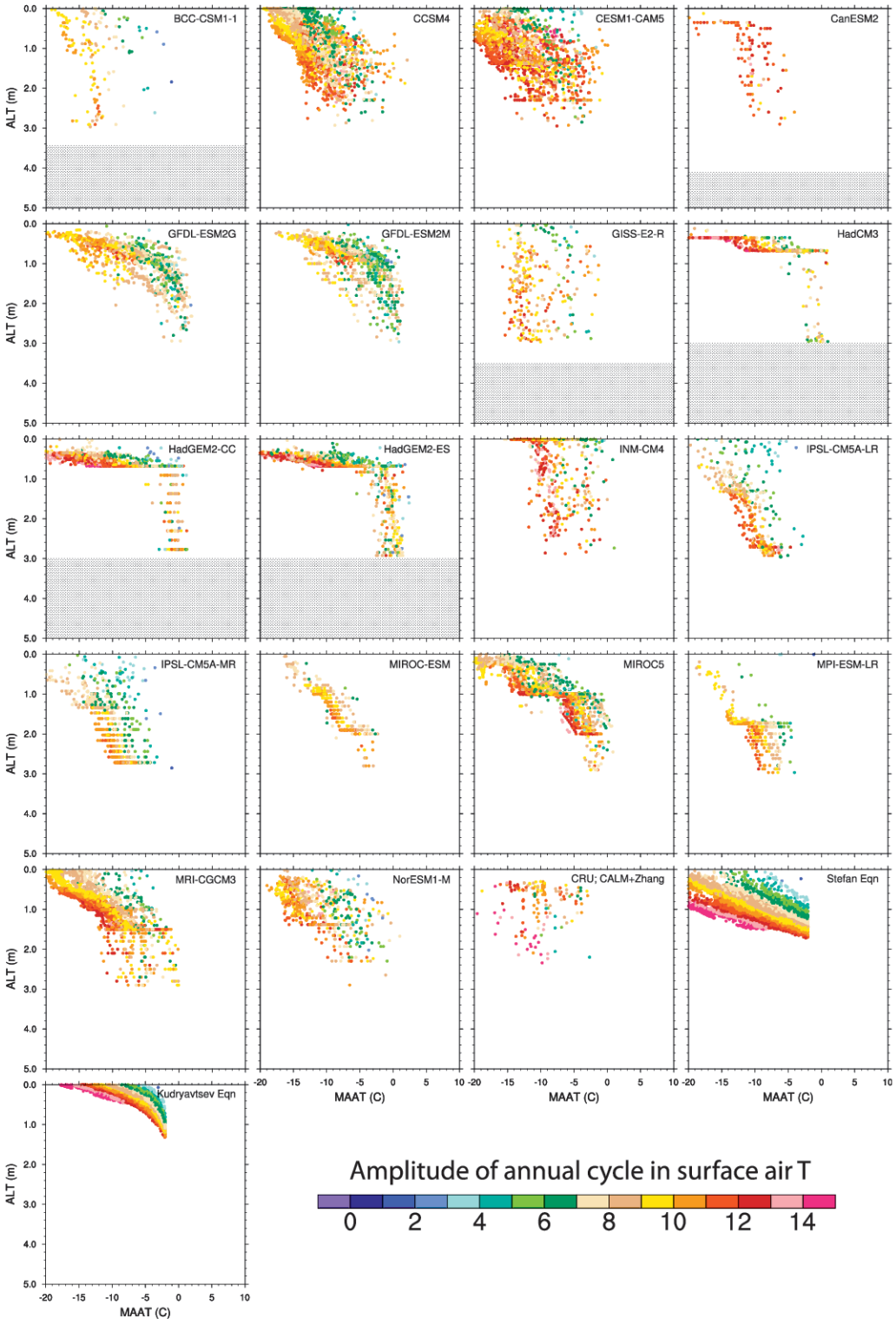

FIG. 3. ALT plotted against MAAT for each of the CMIP5 models and observations. Dots are colored on the basis of the amplitude (½ total seasonal range) of the annual temperature cycle. The gray area at the base of some panels indicates depth beyond that model's vertical domain. Also shown are high-latitude (latitude > 55°N) data from the CALM and Zhang et al. (2006) datasets, with atmospheric climatology defined by the corresponding grid cells of the CRU dataset. The last two panels show two analytic solutions to the heat equation with cyclic upper boundary and phase change (Stefan and Kudryavtsev equations), given a single set of soil thermal properties and CRU climatologies.

TABLE 3. Summary statistics of model–data comparisons. For each column where an observational constrain was available, we assigned a qualitative threshold of the 50% of models that were closest to observations and note these with a boldface type.

Model name	Max depth (m)	Median active layer thickness (m)	Regression constant of trivariate regression (m)	Slope of ALT–MAAT (m °C^{-1})	Slope of ALT–amplitude (m °C^{-1})	r^2 of trivariate regression (unitless)	Mean T offset 0–1 m (°C)	Mean attenuation 0–1 m (unitless)	Mean T offset air–0 m (°C)	Mean attenuation air–0 m (unitless)	RMS error: T offset 0–1 m (°C)	RMS error: attenuation 0–1 m (unitless)	RMS error: T offset air–0 m (°C)	RMS error: attenuation air–0 m (unitless)
BCC-CSM1–1	3.4	1.75	**0.16**	0.253	0.48	**0.41**	**−0.33**	**0.35**	**8.78**	0.29	**0.88**	0.28	**4.28**	**0.33**
CCSM4.0	43.7	1.20	1.23	**0.101**	**0.09**	**0.46**	−1.54	0.25	**7.20**	**0.53**	1.62	0.25	**3.13**	**0.23**
CESM1-CAM5	43.7	1.26	1.46	**0.074**	**0.05**	**0.31**	−1.60	0.30	**8.52**	**0.52**	1.65	**0.21**	**4.51**	**0.22**
CanESM2	4.1	1.38	3.23	0.143	−0.05	**0.39**	**−0.15**	0.71	0.82	**0.84**	**0.84**	0.34	7.14	0.36
GFDL-ESM2G	10.0	0.86	**1.07**	**0.083**	**0.05**	0.55	−1.45	0.57	1.15	0.88	1.34	0.24	5.99	0.35
GFDL-ESM2M	10.0	0.87	**1.20**	**0.097**	**0.04**	0.47	−1.66	**0.48**	0.95	0.86	1.46	**0.16**	6.15	**0.32**
GISS-E2-R	3.5	1.75	**0.31**	**0.042**	0.18	**0.15**	**−0.21**	0.66	**2.81**	**0.55**	**0.80**	0.30	**4.21**	**0.18**
HadCM3	3.0	0.63	**1.17**	**0.053**	0.00	**0.34**	2.06	**0.41**	0.70	0.93	2.99	**0.17**	6.26	0.42
HadGEM2-CC	3.0	0.64	**0.80**	**0.038**	0.02	**0.31**	1.72	**0.46**	0.80	1.01	2.66	**0.15**	6.29	0.47
HadGEM2-ES	3.0	0.64	**1.11**	**0.048**	0.00	**0.34**	1.83	**0.44**	0.89	0.99	2.65	**0.15**	6.23	0.44
INM-CM4	15.0	0.00	**0.36**	0.144	**0.13**	**0.29**	**−0.99**	0.29	**4.04**	**0.42**	**1.00**	0.25	**3.72**	**0.24**
IPSL-CM5A-LR	5.5	2.67	1.57	0.171	0.22	0.77	2.07	0.53	−0.14	1.05	2.91	**0.23**	7.17	0.50
IPSL-CM5A-MR	5.5	2.69	1.70	0.183	0.23	0.80	1.83	0.54	−0.23	1.05	2.56	0.24	7.19	0.50
MIROC-ESM	14.0	1.59	1.99	0.160	**0.08**	0.88	**−0.07**	**0.44**	**3.94**	**0.59**	**0.91**	0.24	**5.29**	**0.27**
MIROC5	14.0	1.00	**1.03**	**0.089**	**0.07**	0.75	**−0.07**	**0.47**	**1.47**	**0.85**	**0.92**	**0.13**	**5.80**	0.35
MPI-ESM-LR	9.6	3.22	1.77	0.172	0.19	0.70	1.18	0.62	−0.01	1.03	1.88	0.28	6.92	0.49
MRI-CGCM3	10.0	1.00	**1.11**	0.108	**0.10**	0.75	**−0.55**	0.33	**6.29**	**0.56**	**0.83**	**0.22**	**3.43**	**0.19**
NorESM1-M	42.1	0.85	1.32	**0.089**	**0.07**	**0.37**	**−1.02**	**0.40**	**7.51**	**0.50**	**1.21**	**0.15**	**3.12**	**0.22**
Observations	—	—	0.32	0.03	0.09	0.13	−0.53	0.40	6.17	0.57	—	—	—	—

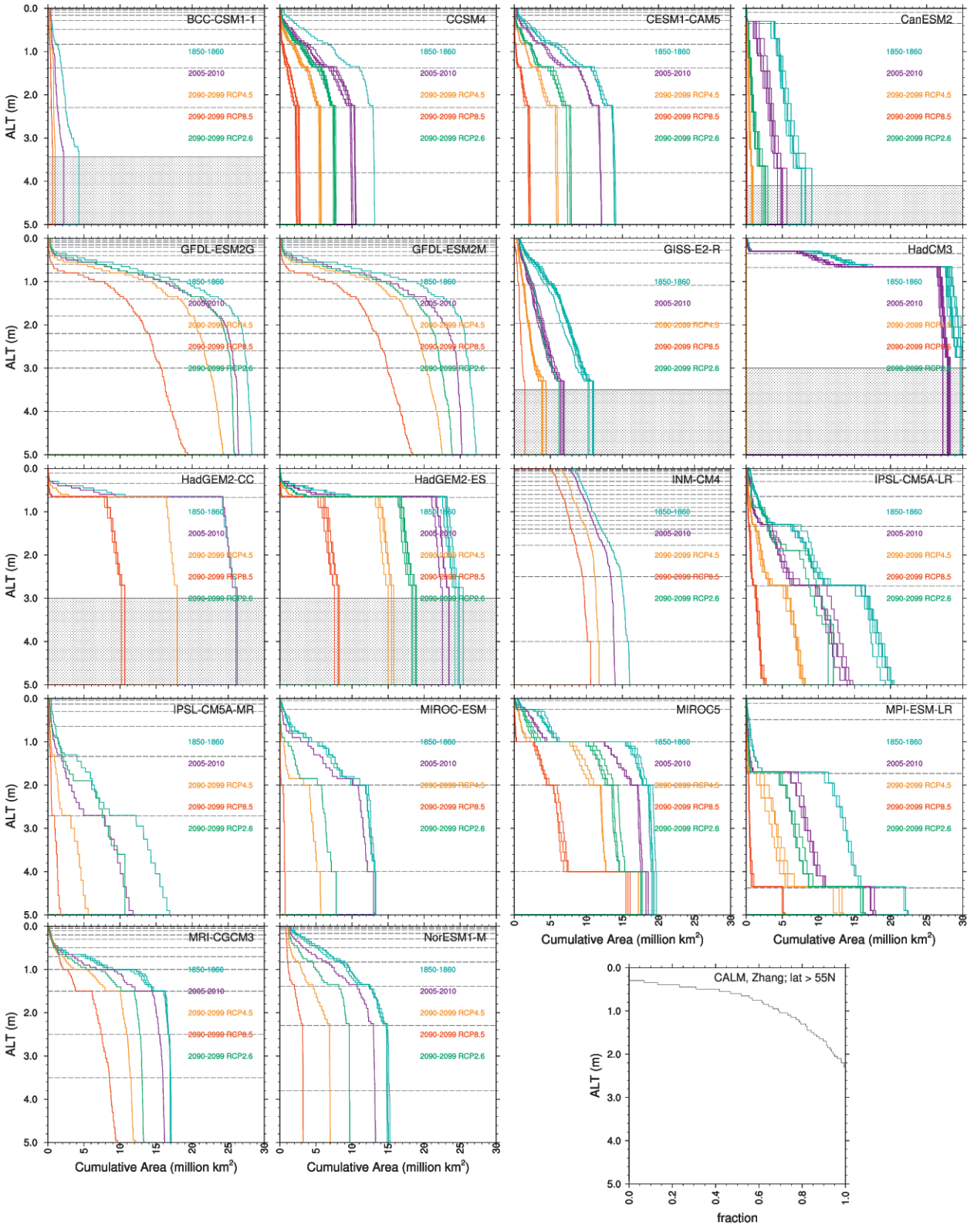

FIG. 4. Cumulative distribution of ALT over the entire modeled permafrost domain in each of the models for historical, current, and future time periods. Also included are observations of current ALT for sites in the CALM and Zhang et al. (2006) datasets north of 55°N, though a direct comparison cannot be made from the observations with the models since the observations have different spatial coverage than the models. Each curve corresponds to the total area (on the horizontal axis) with an active layer less than or equal to the depth (on the vertical axis). Multiple curves for a given time period correspond to individual ensemble members. Model level interfaces are shown as dashed horizontal lines. The gray area at the base of some panels indicates depth beyond that model's vertical domain.

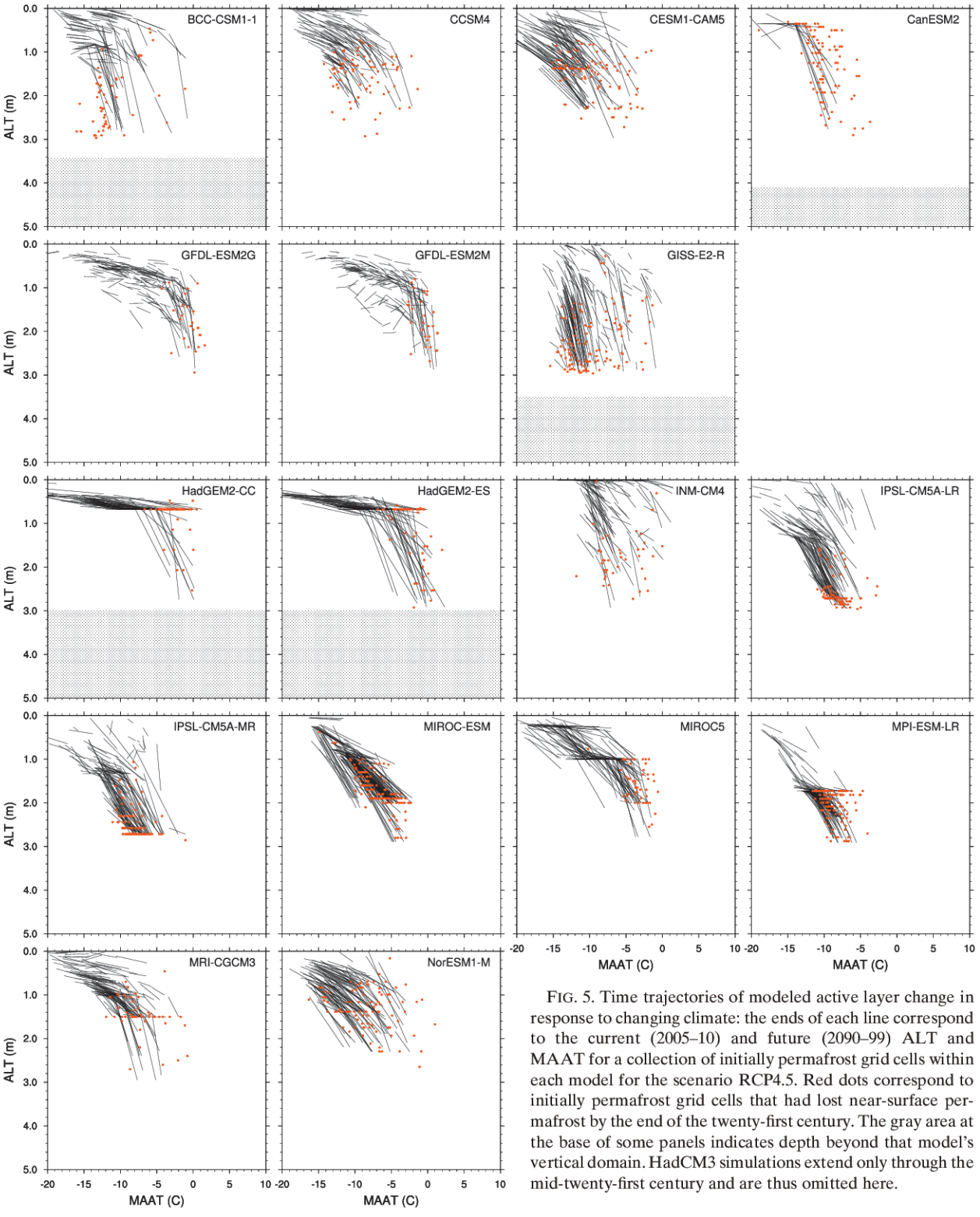

FIG. 5. Time trajectories of modeled active layer change in response to changing climate: the ends of each line correspond to the current (2005–10) and future (2090–99) ALT and MAAT for a collection of initially permafrost grid cells within each model for the scenario RCP4.5. Red dots correspond to initially permafrost grid cells that had lost near-surface permafrost by the end of the twenty-first century. The gray area at the base of some panels indicates depth beyond that model's vertical domain. HadCM3 simulations extend only through the mid-twenty-first century and are thus omitted here.

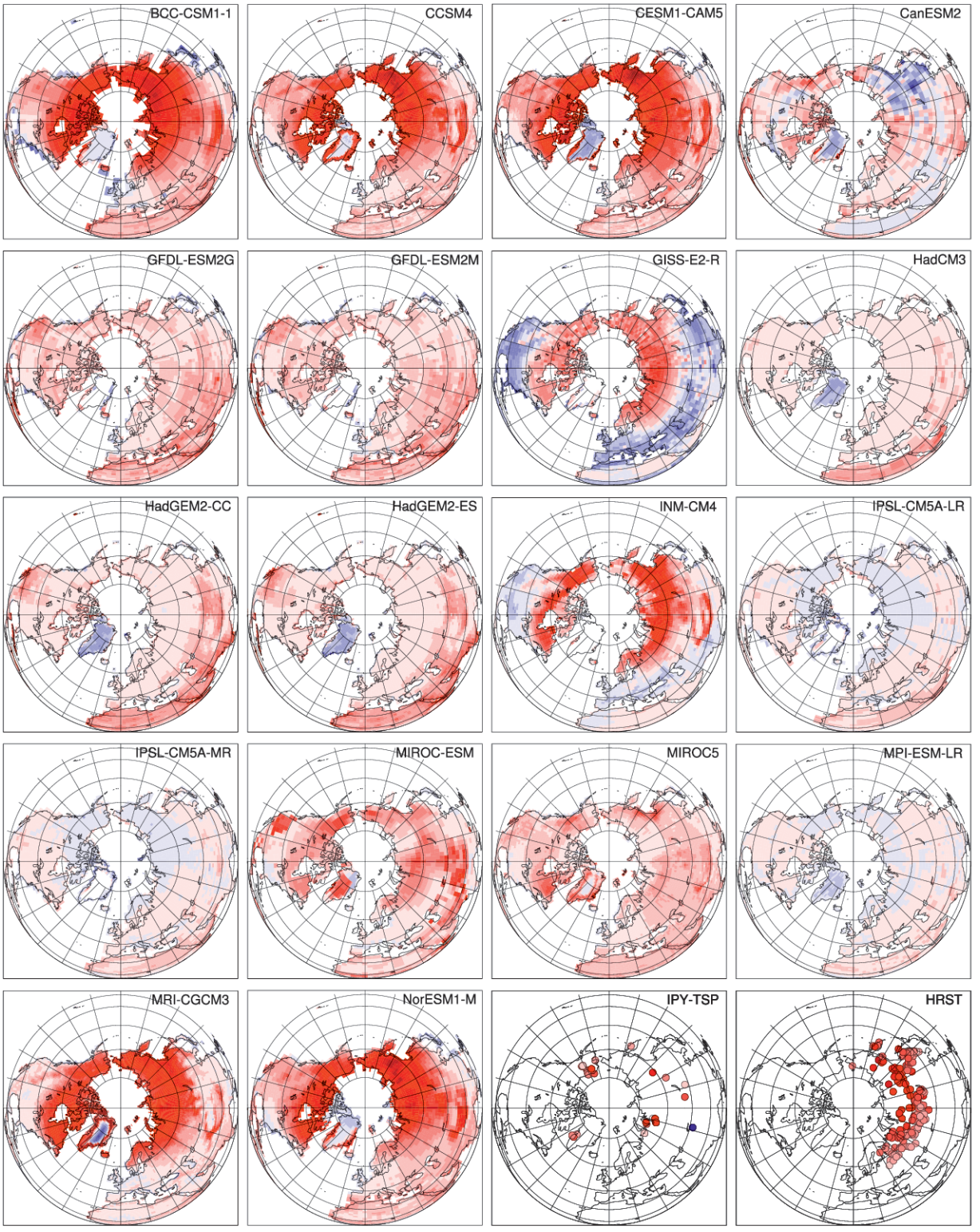

FIG. 6. Maps of $\Delta\overline{T}_{\mathrm{air-0m}}$. Warm colors indicate soil is warmer than air temperature. A major source of the high-latitude temperature offset is from snow insulation effects.

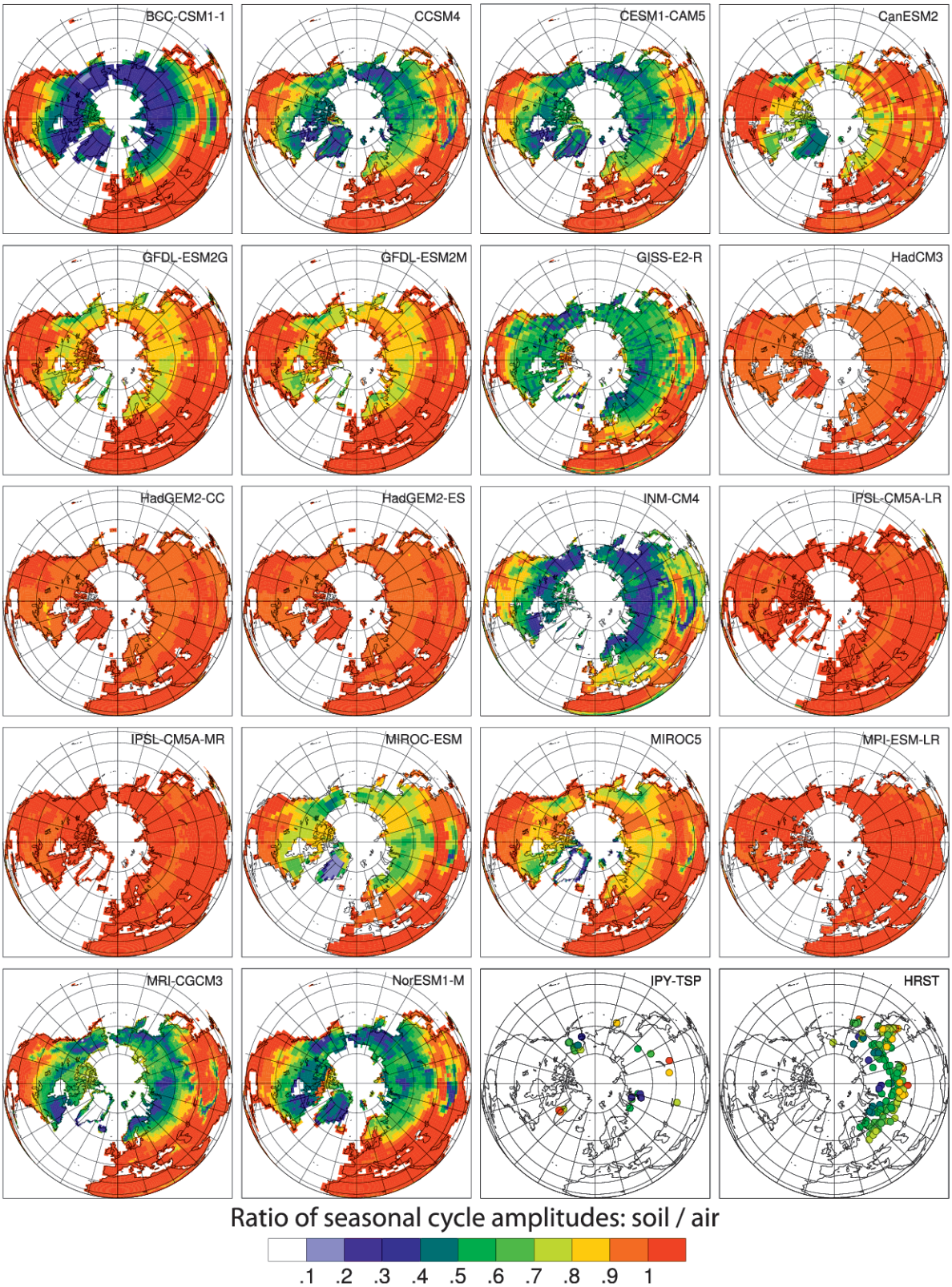

FIG. 7. Maps of $\alpha_{\mathrm{air-0m}}$. As with temperature offset, a major source of high-latitude seasonal-cycle attenuation is from snow insulation effects, and spatial patterns follow those in Fig. 6 closely.

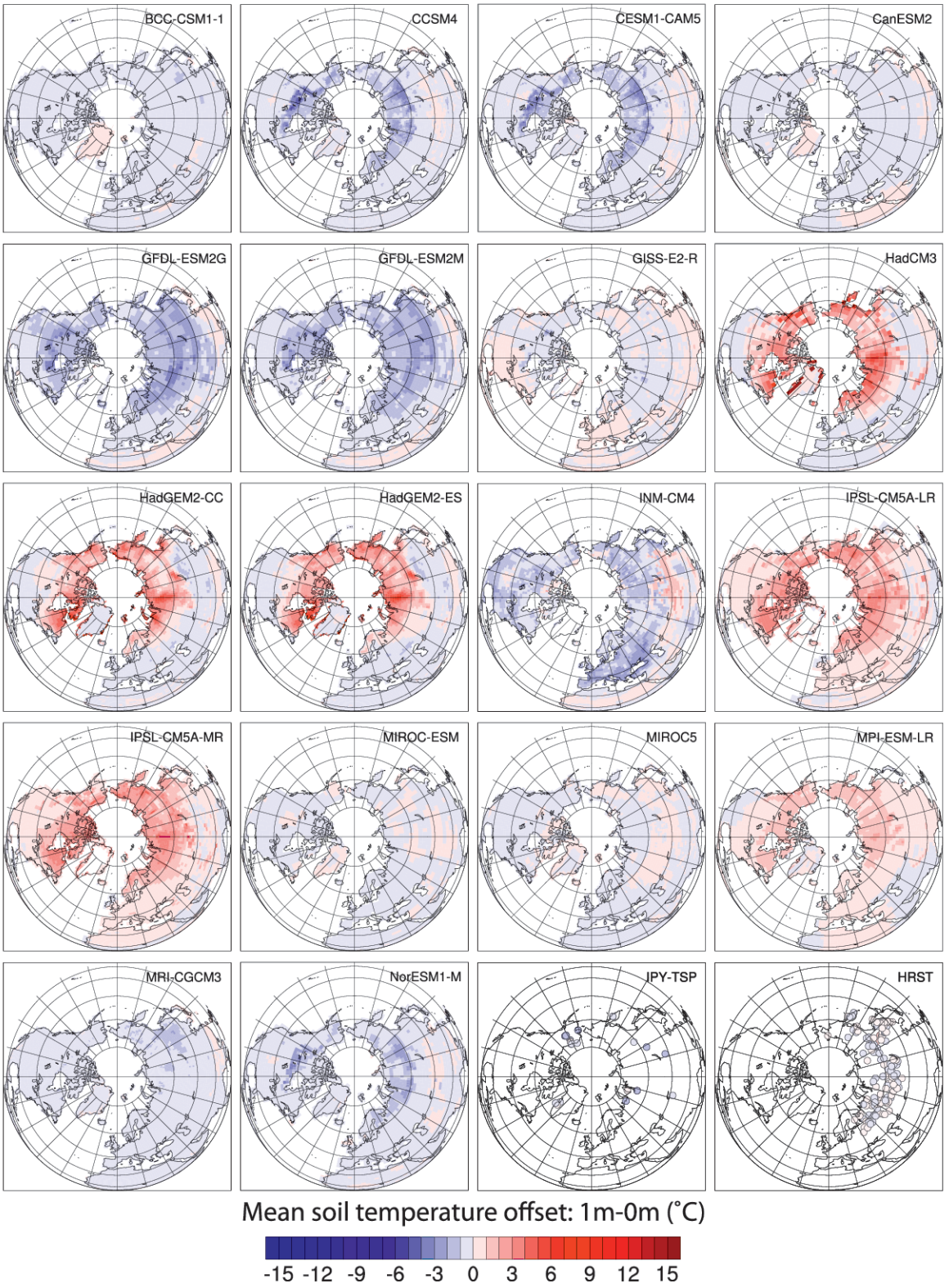

FIG. 8. Maps of $\Delta\overline{T}_{0\mathrm{m}-1\mathrm{m}}$. Warm colors indicate deep soil is warmer than shallow soil. Models with positive (warming) offset all use a snow scheme that substitutes snow for soil thermal properties and thus puts snow insulation effects between soil surface and soil depth (Table 1). Models with negative (cooling) offset show larger influence of differing frozen/unfrozen thermal properties.

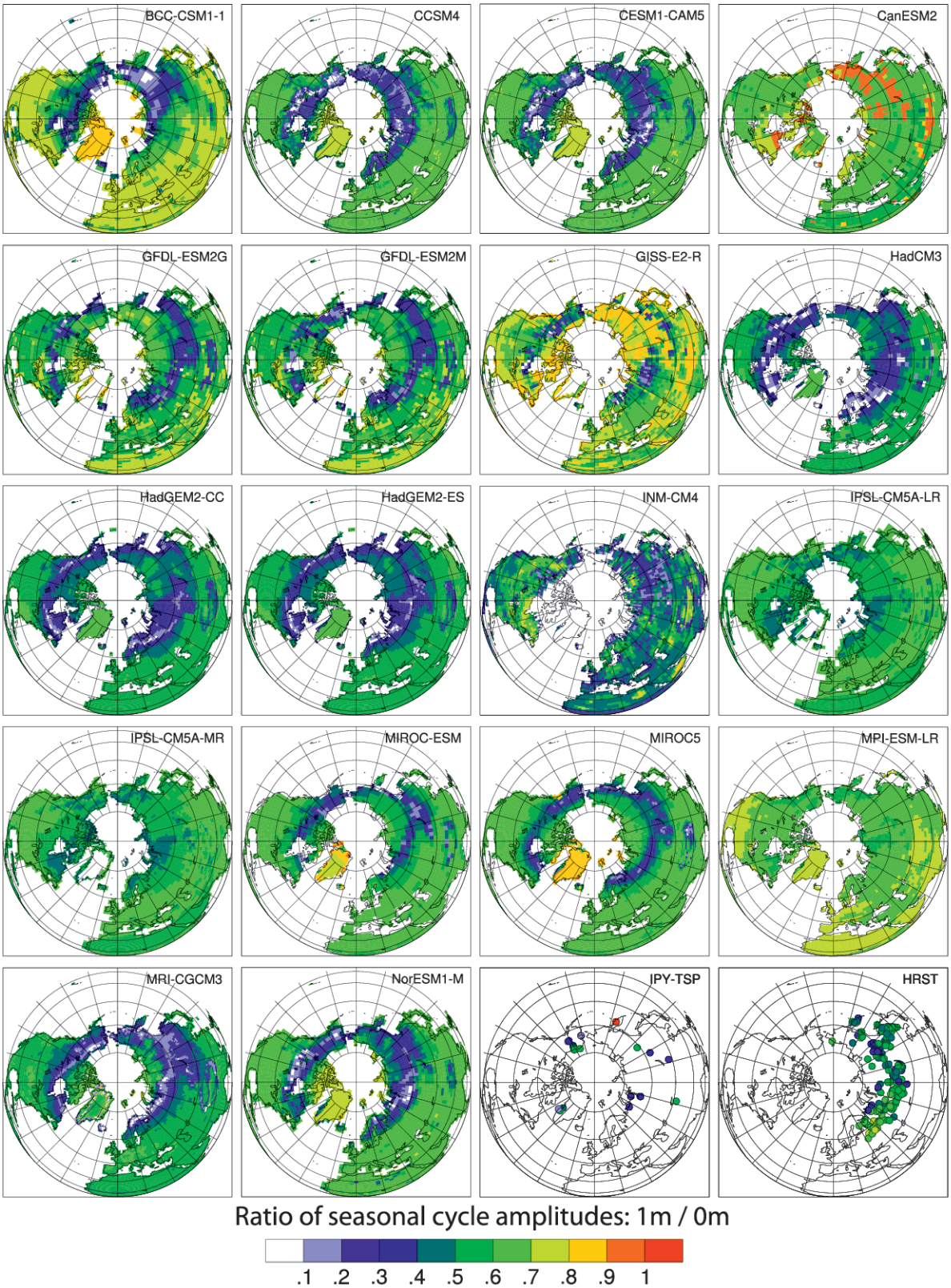

FIG. 9. Maps of α_{0m-1m}. For models that directly couple soil thermal and hydrologic properties, this attenuation is strongly affected by the amount of water that is thawed/frozen during the annual cycle and so is most strong (smallest value of α_{0m-1m}) where soils are wet and active layers are relatively deep.

The change in amplitude through the top meter of soil (α_{0m-1m}, Fig. 9) also shows a strong attenuation (i.e., low values of α_{0m-1m}) throughout the high-latitude region, although its magnitude and spatial distribution vary between models. This signal also shows strongest attenuation across the boreal belt, though the location of the minimum in α_{0m-1m} is typically slightly to the south of the maximum in the air–0m case. In principle, this attenuation should be strongest where the thermal diffusivity (the ratio of the thermal conductivity to the heat capacity) is lowest; if we assume, following the Stefan equation, that the latent heat of fusion of soil water dominates the heat capacity term, then the attenuation should be strongest where the most water changes phase and thus strongest where active layers are as deep as the reference depth and porosity is high. Given that the change in mean temperature with depth through the soils is mostly caused by the differing thermal conductivity between frozen and unfrozen soils (Romanovsky and Osterkamp 1997), this term will be very model dependent but should be strongest (i.e., most negative values of $\Delta\overline{T}_{0m-1m}$) where soil porosity and water content is highest. Unlike for the air–0m interface, the multimodel means in $\Delta\overline{T}_{0m-1m}$ and α_{0m-1m} are only weakly correlated across the models, with an $r^2 = 0.15$. A less strong mean attenuation across the models is also correlated with deeper median active layer thickness ($r^2 = 0.22$, $p = 0.05$). The observations show a pronounced attenuation throughout the permafrost region and a small cooling in the mean soil temperature.

In both the air-to-0m and the 0–1m temperature changes, many of the models fail to reproduce the observed behavior, with many showing less attenuation in the annual cycle amplitude with depth (larger values of α_{0m-1m}) and larger temperature changes (with both warming and cooling with depth predicted in different models). Several of the models, such as the Met Office Surface Exchange Scheme (MOSES)/Top-down Representation of Interactive Foliage and Flora Including Dynamics (TRIFFID) land model in HadGEM2, the Schématisation des Échanges Hydriques à l'Interface Biosphère–Atmosphère (SECHIBA)/Organizing Carbon and Hydrology in Dynamic Ecosystems (ORCHIDEE) land model in IPSL-CM4 [the CMIP5 version of which predates the frozen-soil developments in Poutou et al. (2004) and Koven et al. (2009)], and the Jena Scheme for Biosphere–Atmosphere Coupling in Hamburg (JSBACH) land model in MPI-ESM-LR, show very little warming from the air to the soil, or even cooling, over the high northern latitudes ($\Delta\overline{T}_{air-0m}$, Fig. 6); limited attenuation from air to the soil (α_{air-0m}, Fig. 7); and warming with depth through the soil instead of cooling ($\Delta\overline{T}_{0m-1m}$, Fig. 8). For the HadGEM2, IPSL-CM4, and MPI-ESM models, this lack of attenuation in the α_{air-0m} term is because of the implicit and composite snow treatments (in the sense of Slater et al. 2001), which leads to the models inserting the snow thermal effects between the shallow and deeper soils rather than between the atmosphere and shallow soils. However, differences even among these simplified models are evident: HadGEM2 replaces only the top layer with snow properties while IPSL-CM4 uses snow thermal properties to the depth of the calculated snow thickness, leading to the very different $\Delta\overline{T}_{0m-1m}$ and α_{0m-1m} responses and, consequently, the different permafrost extent and ALT distributions (Figs. 3, 4) between these two models. One advantage in separating the modeled temperature responses into the four components used here ($\Delta\overline{T}_{air-0m}$, $\Delta\overline{T}_{0m-1m}$, α_{air-0m}, and α_{0m-1m}) is that there are possible tradeoffs, such as too-cold soils with too-large amplitudes at depth, that could lead to the same ALT; the separation described here allows for a clearer sense of what controls the permafrost extent and ALT.

A major difference between the models is in their treatment of the latent heat of fusion of soil water (Table 1; Fig. 10), which includes omission, apparent heat capacity over a discrete temperature range, or more detailed thermodynamic treatments of supercooled moisture. A result of these differences can be seen graphically (Fig. 10) by plotting histograms of soil temperatures across a range spanning the soil freezing point. Models that omit latent heat (IPSL-CM5 and MPI-ESM) have a flat distribution; those that include latent heat terms would be expected to show a higher frequency of occurrence through the range that the latent heat term is applied, as a given model grid cell soil level should get stuck at those temperatures for a longer duration during the passage of the seasonal cycle—this is one result of the ''zero-curtain effect'' (Outcalt et al. 1990). The depth at which the zero-curtain effect occurs most strongly also differs between the models and between models and observations. The IPA-IPY and HRST observations, averaged to monthly values and aggregated across all sites within each dataset, show an asymmetric, negatively skewed, relatively gradual peak mainly below the freezing point, as significant unfrozen water exists and continues to freeze well below 0°C. Some of the models (e.g., CLM4) follow this pattern, while others show more sharply peaked distributions centered at a given temperature (which ranges from −2°C to just above 0°C) or multiple peaks corresponding to the boundaries of a discrete range over which an apparent heat capacity is applied [e.g., Meteorological Research Institute Coupled General Circulation Model, version 3 (MRI-CGCM3)]. For the analysis throughout this paper, we have used a cutoff of 0°C for defining the boundary

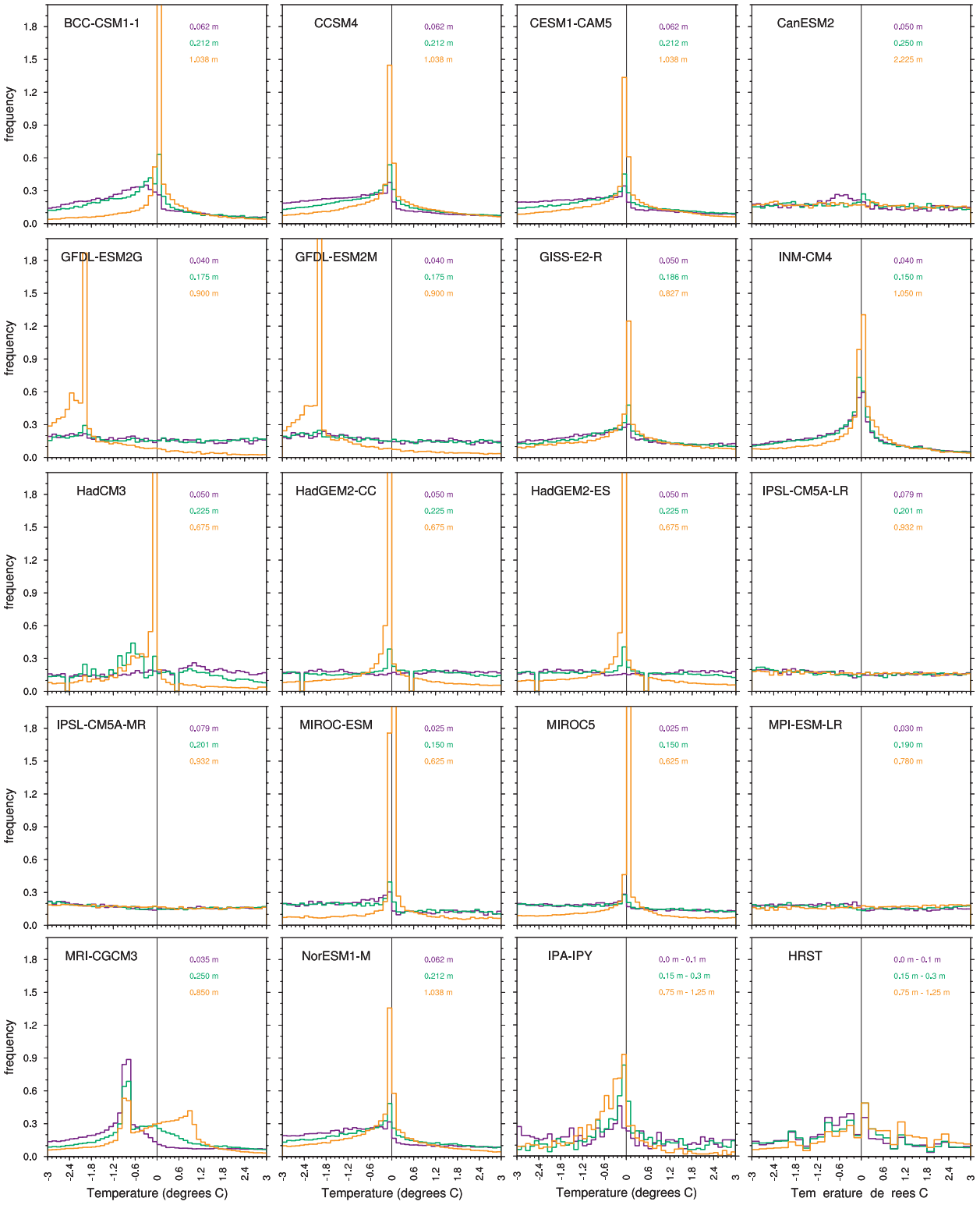

FIG. 10. Histograms of monthly soil temperatures near the freezing point illustrate the effects of differing latent heat parameterization on soil temperatures. For models, all grid cells north of 60°N and the closest model levels to 0.05, 0.2, and 1 m are shown. For IPA-IPY data, daily observations were aggregated to monthly means, and all monthly mean values were used to compute histograms. For HRST data, monthly values of all sites were used. In both sets of observations, all monthly temperatures within the intervals 0–0.1, 0.15–0.3, and 0.75–1.25 m were used. Vertical line in all panels is at 0°C.

between frozen and unfrozen soil and therefore for permafrost; however, this approach may lead to artifacts in models that apply the latent heat term away from zero, such as BCC-CSM1–1, which clusters just above 0°C, or the GFDL models which apply freezing at −2°C.

The amount of coupling between the atmosphere and soil surface, and the mediation of this coupling by snow, has a large impact on the differences between the modeled soil thermal environments. All of the models that simulate high current-climate permafrost extent ($>17 \times 10^6$ km^2) also have low values (<2°C) of $\Delta\overline{T}_{\text{air}-0\text{m}}$, suggesting a first-order control on the modeled permafrost distribution by the air-to-soil thermal offset.

b. Model evaluation

The widely divergent model behavior for these comparisons reflects several underlying causes, including 1) the level of process detail represented in the models, 2) parameter choices, and 3) degree of model calibration. The CMIP5 models are a suite of global atmosphere–ocean–land climate models that must of necessity represent the huge complexity across the earth system. We note that many of these models were not specifically developed to represent permafrost systems, although most modeling groups are actively working to improve this aspect of model performance.

Comparing observations against model predictions for the metrics defined above indicates no clear ranking of the models (Tables 2, 3). For the soil thermal comparisons (Table 3), the rankings based on the modeled mean response at the observation sites are largely the same as the rankings based on the RMS error, showing that it is the intermodel differences in the mean response that dominate the RMS term rather than the model differences in the intersite correlation. This conclusion is supported by the fairly uniform high-latitude signals in the thermal metrics (Figs. 6–9).

c. Comparison of modeled permafrost response to warming

While all of the models show some loss of permafrost under twenty-first century warming, the range of responses is large for all RCP scenarios (Fig. 11; Table 2). There are two ways of looking at the changes to modeled permafrost extent: as absolute changes to the permafrost area or, given that there are such large differences in the initial permafrost distributions between the models, as fractional changes to permafrost area. If we look at the absolute changes, then they range from 0.1 to 5.2 million km^2 for RCP2.6, 0.6 to 8.0 million km^2 for RCP4.5, and 0.9 to 15.7 million km^2 for RCP8.5. The fractional loss in permafrost extent between 2005 and 2100 ranges from 2% to 66% for RCP2.6, 15% to 87% for RCP4.5, and 30% to 99% for RCP8.5. Despite these large ranges and their implied model uncertainty, the range of model responses can be used to offer some implications for permafrost under climate change: for example, these models predict much more drastic losses in permafrost under the high-warming scenarios RCP4.5 and, especially, RCP8.5 than under the low-warming RCP2.6 scenario.

Given that the CMIP5 models are all fully coupled land–atmosphere–ocean models and our analysis only covers the surface air–soil domain, we expect large intermodel differences associated with other climate forcings, such as a model's overall climate sensitivity and degree of arctic amplification. To separate these differences from those associated with the surface air–soil domain, we calculate absolute and relative permafrost vulnerability indices as the ratio of the absolute or fractional extent of permafrost loss to the total high-latitude climate temperature change. Here we define high-latitude climate change as change in MAAT over land, oceans, and ice poleward of 60°N. Using the RCP4.5 scenario, the CMIP5 models have absolute permafrost vulnerability indices of 0.2–3.5 million km^2 permafrost per 1°C high-latitude warming and fractional vulnerability indices that range from 6% to 29% °C^{-1} (Table 2). For the absolute vulnerability index, much of this range is set by outlier models at either end of the sensitivity range: for the models as a set, the mean and standard deviation of this value is 1.6 ± 0.7 million km^2 permafrost per 1°C high-latitude warming, and for the fractional loss the ensemble mean is 13% ± 6% permafrost loss per 1°C high-latitude warming.

Ideally, in this type of multimodel climate change analysis, one would like to find a metric that is both observable within the current climate and has predictive power over the system's response to transient climate change (Hall and Qu 2006). One such relationship, at the scale of individual grid cells, can be seen by the similarity between Figs. 3 and 5: the models' predictions of climate control of ALT at the present day inform their predictions of ALT response to changing climate. At the panarctic scale, the choice of metric dictates the control variable, because across the set of models, the two vulnerability indices (absolute and fractional) are not correlated ($r^2 < 0.001$). The absolute permafrost vulnerability is largely controlled by the initial permafrost area ($r^2 = 0.41$, $p < 0.01$), while the fractional vulnerability index is negatively correlated with initial permafrost area ($r^2 = 0.48$, $p < 0.01$) and positively correlated with median present-day active layer thickness ($r^2 = 0.27$, $p < 0.05$).

While many processes (such as those listed in Table 1) are treated differently or with varying degrees of

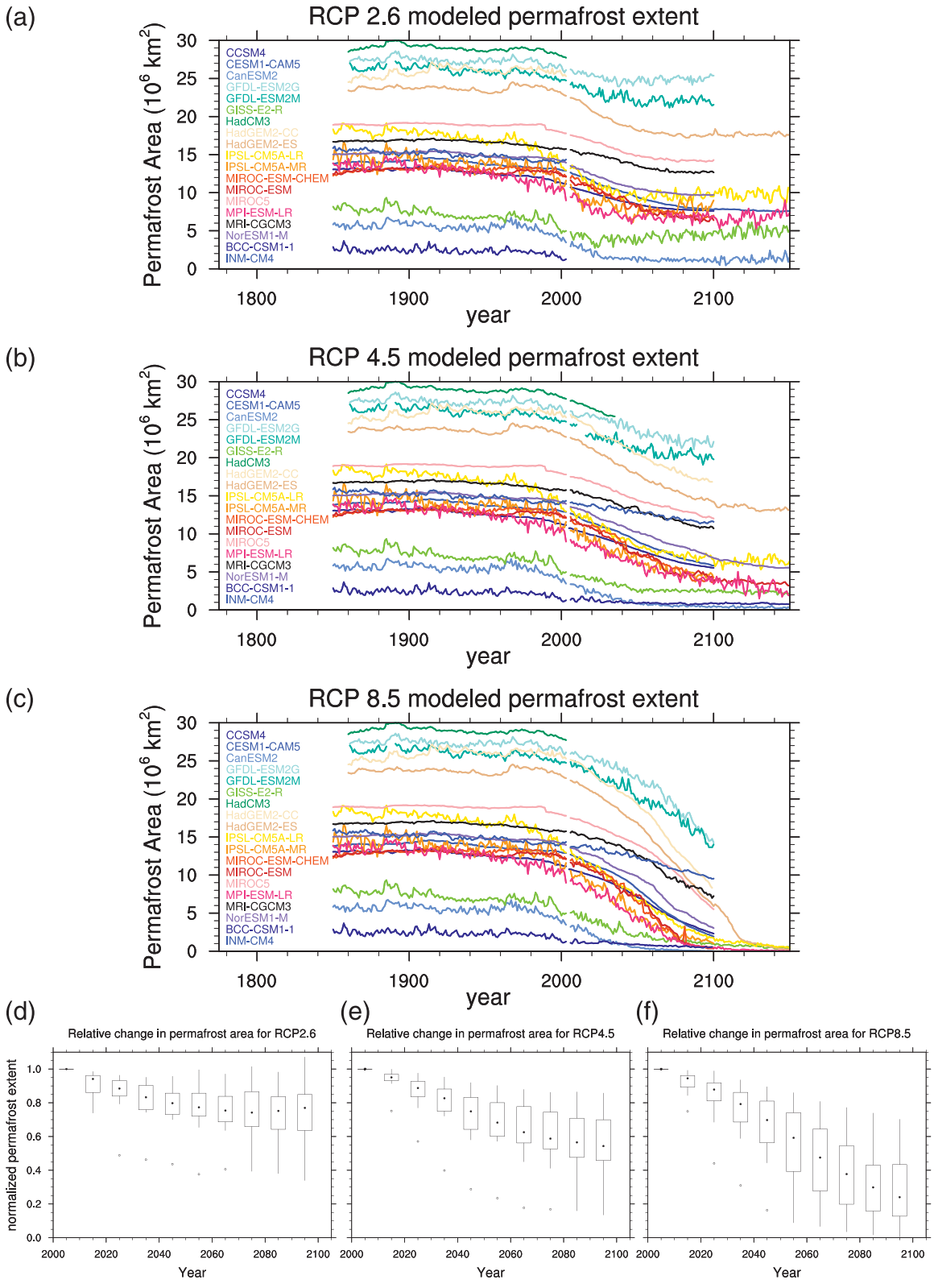

FIG. 11. Multimodel predictions of permafrost area under climate change scenarios: (a),(d) RCP2.6, (b),(e) RCP4.5, and (c),(f) RCP8.5. Total permafrost extent for each model in CMIP5 analysis is shown in (a)–(c). A small gap is shown between historical experiment and RCP scenarios. Box–whisker diagrams of fraction of permafrost at start of RCP scenarios remaining during the twenty-first century are shown in (d)–(f).

complexity, in these models they share many common characteristics. In addition to what they share in terms of resolved processes, they share a lack of other processes known to be important in permafrost dynamics, including 1) processes that could act to accelerate permafrost loss with warming, such as thermokarst and the lateral thaw associated with finescale coupling of thermal and hydrologic properties, and 2) processes that could act to slow permafrost loss with warming, including the presence of massive ground ice which would need to melt in order to substantially deepen active layers.

The lack of representation of these critical processes in any of the CMIP5 models in combination with 1) the wide range of model predictions of ALT and permafrost extent under current and projected climate and 2) relatively poor comparisons with observed permafrost thermal properties (e.g., none of the models performed well in every comparison with the data) lead us to conclude that, as a group, the current suite of CMIP5 model projections of permafrost loss and dynamics over the coming century is very uncertain. Given that these dynamics are closely linked to prediction of the potential CO_2 and CH_4 emissions and resulting atmospheric feedbacks, we argue that model projections of high-latitude C cycle climate feedbacks over the next century based on the physics in these models (even beyond the fact that a permafrost C cycle is not represented in any of these simulations) are also very uncertain.

4. Summary and conclusions

We compare permafrost thermal dynamics for a set of models participating in the CMIP5 project to evaluate their behavior under the current climate and assess the range of model predictions for permafrost extent under transient global warming experiments. The models show a wide range of behaviors under the current climate, with many failing to agree with fundamental aspects of the observed soil thermal regime at high latitudes.

Under future climate change, the models differ in their degree of warming, both globally and at high latitudes, and also in the response of permafrost to this warming. All of the models show some loss of permafrost, but there is a wide range of possible magnitudes in their responses, from 6% to 29% permafrost loss per 1°C high-latitude warming. Several of the models predict that substantial permafrost degradation has already occurred (ranging from 3% gain to 49% loss relative to 1850 conditions), though the majority of models at the high end of relative twentieth-century permafrost loss also show unrealistically small preindustrial permafrost extent; given that such high rates of permafrost loss are not observed, this indicates a too-high sensitivity for those models predicting such losses.

Given the large complexity and number of differing components of the CMIP5 models, we find that a useful approach to understand the model differences is to break down the thermal communication between the surface air and deeper soil by examining changes to the mean and amplitude of the annual temperature cycle across the air to surface soil and surface soil to deeper soil interfaces. The available soil temperature observations at high latitudes allow such an observational constraint and demonstrate that different model representations lead to better or worse agreement with different aspects of the observed soil thermal climate.

Much of the disagreement in modeled mean soil temperatures can be traced to the representation of thermal connection between the air and land surface and, in particular, its mediation by snow in winter. There is wide model disagreement on the value of $\Delta\overline{T}_{\mathrm{air-0m}}$, the difference in mean temperatures across the air–soil interface, with several of the models predicting the wrong sign for this statistic. Similarly, there is wide model disagreement in the changes of mean and amplitude of soil temperatures with depth, some of which can be tied to differences in modeled soil physical properties and coupling between soil temperature and hydrology. This appears to be particularly the case for the representation of organic layers; even models that do incorporate organic material do so using a mixture of organic and mineral properties instead of representing organic soils as separate units, with their own dynamics distinct from mineral soils. Models that show deep active layers under the current climate are more likely to have larger fractional reductions in their fractional permafrost extent with warming.

Given that the high-latitude soil C pool is the single largest component of the terrestrial carbon cycle that could respond directly to climate change on time scales of centuries, it is important for ESMs to accurately predict how the permafrost soil climate may respond to warming. With this analysis, we show that widespread disagreement exists among this generation of ESMs. All CMIP5 models predict some loss of permafrost, and increasing loss under higher-warming scenarios, but the magnitude of this loss is still highly uncertain.

Acknowledgments. This research was supported by the Director of the Office of Biological and Environmental Research, Office of Science, U.S. Department of Energy, under Contract DE-AC02-05CH11231 as part of the Regional and Global Climate Modeling Program (RGCM). We acknowledge the World Climate Research

Programme's Working Group on Coupled Modelling, which is responsible for CMIP, and we thank the climate modeling groups (listed in Table 1 of this paper) for producing and making available their model output. Thanks to Igor Aleinov, Eleanor Burke, Stefan Hagemann, Masahiro Hosaka, Weiping Li, Chris Milly, Kazuyuki Saito, Diana Verseghy, and Evgeny Volodin for information on the model structures reported in Table 1. For CMIP the U.S. Department of Energy's Program for Climate Model Diagnosis and Intercomparison provided coordinating support and led development of software infrastructure in partnership with the Global Organization for Earth System Science Portals. Thanks to Vladimir Romanovsky for helpful discussion and for sharing IPY-TSP data and to Andrew Slater and David Lawrence for helpful discussion.

REFERENCES

Brown, J., O. Ferrians Jr., J. Heginbottom, and E. Melnikov, 1998: Circum-Arctic map of permafrost and ground-ice conditions. National Snow and Ice Data Center, Boulder, CO, digital media. [Available online at http://nsidc.org/data/docs/fgdc/ggd318_map_circumarctic/index.html.]

——, K. Hinkel, and F. Nelson, 2000: The Circumpolar Active Layer Monitoring (CALM) program: Research designs and initial results. *Polar Geogr.,* **24,** 165–258, doi:10.1080/10889370009377698.

Burke, E. J., I. P. Hartley, and C. D. Jones, 2012: Uncertainties in the global temperature change caused by carbon release from permafrost thawing. *Cryosphere Discuss.,* **6,** 1367–1404, doi:10.5194/tcd-6-1367-2012.

Burn, C. R., and F. E. Nelson, 2006: Comment on "A projection of severe near-surface permafrost degradation during the 21st century" by David M. Lawrence and Andrew G. Slater. *Geophys. Res. Lett.,* **33,** L21503, doi:10.1029/2006GL027077.

Ciais, P., and Coauthors, 2012: Large inert carbon pool in the terrestrial biosphere during the last glacial maximum. *Nat. Geosci.,* **5,** 74–79, doi:10.1038/ngeo1324.

Cox, P., R. Betts, C. Bunton, R. Essery, P. Rowntree, and J. Smith, 1999: The impact of new land surface physics on the GCM simulation of climate and climate sensitivity. *Climate Dyn.,* **15,** 183–203.

DeConto, R. M., S. Galeotti, M. Pagani, D. Tracy, K. Schaefer, T. Zhang, D. Pollard, and D. J. Beerling, 2012: Past extreme warming events linked to massive carbon release from thawing permafrost. *Nature,* **484,** 87–91, doi:10.1038/nature10929.

Dunnea, J. P., and Coauthors, 2012: GFDL's ESM2 global coupled climate–carbon earth system models. Part I: Physical formulation and baseline simulation characteristics. *J. Climate,* **25,** 6646–6665.

Essery, R., M. Best, R. Betts, P. Cox, and C. Taylor, 2003: Explicit representation of subgrid heterogeneity in a GCM land surface scheme. *J. Hydrometeor.,* **4,** 530–543.

Gilichinsky, D., R. Barry, S. Bykhovets, V. Sorokovikov, T. Zhang, S. Zudin, and D. Fedorov-Davydov, 1998: A century of temperature observations of soil climate: Methods of analysis and long-term trends. *Proc. Seventh Int. Conf. on Permafrost,* Yellowknife, Northwest Territories, Canada, International Permafrost Association, 23–27.

Hall, A., and X. Qu, 2006: Using the current seasonal cycle to constrain snow albedo feedback in future climate change. *Geophys. Res. Lett.,* **33,** L03502, doi:10.1029/2005GL025127.

Harden, J. W., and Coauthors, 2012: Field information links permafrost carbon to physical vulnerabilities of thawing. *Geophys. Res. Lett.,* **39,** L15704, doi:10.1029/2012GL051958.

Hinzman, L., D. Goering, and D. Kane, 1998: A distributed thermal model for calculating soil temperature profiles and depth of thaw in permafrost regions. *J. Geophys. Res.,* **103** (D22), 28 975–28 991.

Holland, M. M., and C. M. Bitz, 2003: Polar amplification of climate change in coupled models. *Climate Dyn.,* **21,** 221–232, doi:10.1007/s00382-003-0332-6.

Ji, J., 1995: A climate-vegetation interaction model: Simulating physical and biological processes at the surface. *J. Biogeogr.,* **22,** 445–451.

Koven, C. D., P. Friedlingstein, P. Ciais, D. Khvorostyanov, G. Krinner, and C. Tarnocai, 2009: On the formation of high-latitude soil carbon stocks: The effects of cryoturbation and insulation by organic matter in a land surface model. *Geophys. Res. Lett.,* **36,** L21501, doi:10.1029/2009GL040150.

——, B. Ringeval, P. Friedlingstein, P. Ciais, P. Cadule, D. Khvorostyanov, G. Krinner, and C. Tarnocai, 2011: Permafrost carbon-climate feedbacks accelerate global warming. *Proc. Natl. Acad. Sci. USA,* **108,** 14 769–14 774, doi:10.1073/pnas.1103910108.

Krinner, G., and Coauthors, 2005: A dynamic global vegetation model for studies of the coupled atmosphere-biosphere system. *Global Biogeochem. Cycles,* **19,** GB1015, doi:10.1029/2003GB002199.

Lawrence, D. M., and A. G. Slater, 2005: A projection of severe near-surface permafrost degradation during the 21st century. *Geophys. Res. Lett.,* **32,** L24401, doi:10.1029/2005GL025080.

——, and ——, 2008: Incorporating organic soil into a global climate model. *Climate Dyn.,* **30,** 145–160, doi:10.1007/s00382-007-0278-1.

——, and Coauthors, 2011: Parameterization improvements and functional and structural advances in version 4 of the community land model. *J. Adv. Model. Earth Syst.,* **3,** M03001, doi:10.1029/2011MS000045.

——, A. G. Slater, and S. C. Swenson, 2012: Simulation of present-day and future permafrost and seasonally frozen ground conditions in CCSM4. *J. Climate,* **25,** 2207–2225.

Luo, Y. Q., and Coauthors, 2012: A framework of benchmarking land models. *Biogeosci. Discuss.,* **9,** 1899–1944, doi:10.5194/bgd-9-1899-2012.

Mitchell, T. D., and P. D. Jones, 2005: An improved method of constructing a database of monthly climate observations and associated high-resolution grids. *Int. J. Climatol.,* **25,** 693–712, doi:10.1002/joc.1181.

Nicolsky, D. J., V. E. Romanovsky, V. A. Alexeev, and D. M. Lawrence, 2007: Improved modeling of permafrost dynamics in a GCM land-surface scheme. *Geophys. Res. Lett.,* **34,** L08501, doi:10.1029/2007GL029525.

——, ——, and G. G. Panteleev, 2009: Estimation of soil thermal properties using in-situ temperature measurements in the active layer and permafrost. *Cold Reg. Sci. Technol.,* **55,** 120–129, doi:10.1016/j.coldregions.2008.03.003.

Outcalt, S., F. Nelson, and K. Hinkel, 1990: The zero-curtain effect: Heat and mass-transfer across an isothermal region in freezing soil. *Water Resour. Res.,* **26,** 1509–1516.

Poutou, E., G. Krinner, C. Genthon, and N. de Noblet-Ducoudre, 2004: Role of soil freezing in future boreal climate change. *Climate Dyn.,* **23,** 621–639, doi:10.1007/s00382-004-0459-0.

Raddatz, T. J., and Coauthors, 2007: Will the tropical land biosphere dominate the climate–carbon cycle feedback during the twenty-first century? *Climate Dyn.,* **29,** 565–574, doi:10.1007/s00382-007-0247-8.

Rinke, A., P. Kuhry, and K. Dethloff, 2008: Importance of a soil organic layer for Arctic climate: A sensitivity study with an Arctic RCM. *Geophys. Res. Lett.,* **35,** L13709, doi:10.1029/2008GL034052.

Riseborough, D., N. Shiklomanov, B. Etzelmuller, S. Gruber, and S. Marchenko, 2008: Recent advances in permafrost modelling. *Permafrost Periglacial Processes,* **19,** 137–156, doi:10.1002/ppp.615.

Romanovsky, V. E., 2010: Development of a network of permafrost observatories in North America and Russia: The US contribution to the international polar year. Advanced Cooperative Arctic Data and Information Service, Boulder, CO, digital media. [Available online at http://www.aoncadis.org/dataset/org.nsf.aon.cadis.Hydrology_and_Terrestrial_Cryosphere.Permafrost_Observatories.html.]

——, and T. E. Osterkamp, 1997: Thawing of the active layer on the coastal plain of the Alaskan arctic. *Permafrost Periglacial Processes,* **8,** 1–22.

——, S. L. Smith, and H. H. Christiansen, 2010: Permafrost thermal state in the polar Northern Hemisphere during the international polar year 2007–2009: A synthesis. *Permafrost Periglacial Processes,* **21,** 106–116, doi:10.1002/ppp.689.

Rosenzweig, C., and F. Abramopoulos, 1997: Land-surface model development for the GISS GCM. *J. Climate,* **10,** 2040–2054.

Schaefer, K., T. Zhang, A. G. Slater, L. Lu, A. Etringer, and I. Baker, 2009: Improving simulated soil temperatures and soil freeze/thaw at high-latitude regions in the Simple Biosphere/Carnegie-Ames-Stanford Approach model. *J. Geophys. Res.,* **114,** F02021, doi:10.1029/2008JF001125.

——, ——, L. Bruhwiler, and A. P. Barrett, 2011: Amount and timing of permafrost carbon release in response to climate warming. *Tellus,* **63B,** 165–180, doi:10.1111/j.1600-0889.2011.00527.x.

Schneider von Deimling, T., M. Meinshausen, A. Levermann, V. Huber, K. Frieler, D. M. Lawrence, and V. Brovkin, 2012: Estimating the near-surface permafrost-carbon feedback on global warming. *Biogeosciences,* **9,** 649–665, doi:10.5194/bg-9-649-2012.

Shiklomanov, N. I., O. A. Anisimov, T. Zhang, S. Marchenko, F. E. Nelson, and C. Oelke, 2007: Comparison of model-produced active layer fields: Results for northern Alaska. *J. Geophys. Res.,* **112,** F02S10, doi:10.1029/2006JF000571.

Slater, A. G., and D. M. Lawrence, 2013: Diagnosing present and future permafrost from climate models. *J. Climate,* in press.

——, and Coauthors, 2001: The representation of snow in land surface schemes: Results from PILPS 2(d). *J. Hydrometeor.,* **2,** 7–25.

Stine, A. R., P. Huybers, and I. Y. Fung, 2009: Changes in the phase of the annual cycle of surface temperature. *Nature,* **457,** 435–440, doi:10.1038/nature07675.

Takata, K., S. Emori, and T. Watanabe, 2003: Development of the minimal advanced treatments of surface interaction and runoff. *Global Planet. Change,* **38,** 209–222, doi:10.1016/S0921-8181(03)00030-4.

Tarnocai, C., J. G. Canadell, E. A. G. Schuur, P. Kuhry, G. Mazhitova, and S. Zimov, 2009: Soil organic carbon pools in the northern circumpolar permafrost region. *Global Biogeochem. Cycles,* **23,** GB2023, doi:10.1029/2008GB003327.

Taylor, K. E., R. J. Stouffer, and G. A. Meehl, 2009: A summary of the CMIP5 experiment design. PCMDI Tech. Rep., 33 pp. [Available online at http://cmip-pcmdi.llnl.gov/cmip5/docs/Taylor_CMIP5_design.pdf.]

USDA Soil Survey Staff, 1998: *Keys to Soil Taxonomy*. 8th ed. U.S. Dept. of Agriculture, Washington, DC, 326 pp.

Verseghy, D. L., 1991: CLASS—A Canadian land surface scheme for GCMS. I. Soil model. *Int. J. Climatol.,* **11,** 111–133.

Volodin, E., N. Dianskii, and A. Gusev, 2010: Simulating present-day climate with the INMCM4.0 coupled model of the atmospheric and oceanic general circulations. *Atmos. Oceanic Phys.,* **46,** 414–431, doi:10.1134/S000143381004002X.

Yukimoto, S., and Coauthors, 2012: A new global climate model of the meteorological research institute: MRI-CGCM3 – Model description and basic performance. *J. Meteor. Soc. Japan,* **90A,** 23–64, doi:10.2151/jmsj.2012-A02.

Zhang, T., R. Barry, and D. Gilichinsky, 2001: Russian historical soil temperature data. National Snow and Ice Data Center, Boulder, CO, digital media. [Available online at http://nsidc.org/data/arcss078.html.]

——, O. W. Frauenfeld, and R. G. Barry, 2006: Time series of active layer thickness in the Russian Arctic, 1930–1990. National Snow and Ice Data Center, Boulder, CO, digital media. [Available online at http://nsidc.org/data/arcss160.html.]